Departamento de Astrofísica
Universidad de La Laguna

M.Sc. in Astrophysics
MASTER'S THESIS

Empirical assessment of proposed mechanisms to explain the presence of CNO processed material in the surface of slowly rotating massive stars.

Supervisor: Dr. Sergio Simón Díaz
Author: Alejandro Santos García

June 2022
San Cristóbal de La Laguna

Resumen

En este trabajo de Fin de Máster se estudiarán distintos procesos que tienen lugar en el interior de estrellas masivas de tipo OB para tratar de explicar el motivo por el cual algunas de estas estrellas tienen una abundancia de nitrógeno en la superficie estelar mayor de lo esperado.

El trabajo está dividido en cuatro partes, siendo la primera una *introducción* al campo de las estrellas masivas y los antecedentes que han llevado a que sea interesante realizar este estudio a día de hoy. Las estrellas masivas de tipo OB han sido objeto de investigación durante décadas ya que, debido a su corta vida, son una gran fuente de información del medio en el que se encuentran. Ya a finales del siglo pasado se observó que algunas de estas estrellas tenían una abundancia de nitrógeno en la superficie mayor a la que se esperaría. Estaba teniendo lugar una transferencia de materia desde el núcleo estelar hasta la superficie, y los materiales obtenidos mediante la quema de H en He en el núcleo mediante el denominado ciclo CNO estaban siendo observados en la superficie. Las estrellas de alta masa tienen núcleos convectivos y envolturas radiativas, por lo que no se espera que el material del núcleo alcance la superficie. Las primeras teorías parecían indicar que esto estaba pasando debido a procesos de mezcla por la generación de corrientes meridionales debidas a la alta rotación que llegan a alcanzar estas estrellas (Meynet & Maeder, 2000; Heger & Langer, 2000), pero la aparición de nuevos datos gracias a las observaciones llevadas a cabo por el proyecto VLT/FLAMES Survey of Massive Stars (P.I. S. Smartt) parecía contradecir lo supuesto hasta entonces. Las nuevas observaciones encontraron estrellas masivas de tipo OB cuya abundancia de nitrógeno era alta en la superficie, pero la velocidad de rotación proyectada, $v \sin i$, medida era muy baja como para que está fuera la explicación del enriquecimiento de nitrógeno (Hunter et al., 2008). Se llevaron a cabo distintos estudios para tratar de entender que estaba pasando en este tipo de estrellas con baja velocidad de rotación. Algunos mecanismos que podrían tener lugar en el interior de la estrella y que podrían producir esto serían la presencia de campos

magnéticos (Morel et al., 2008; Przybilla & Nieva, 2011) o con las oscilaciones que tienen lugar en el interior de la estrella (Aerts et al., 2014). Además, otra cosa a tener en cuenta es que se ha encontrado que un alto porcentaje de estrellas masivas evolucionan como parte de sistemas binarios (Sana et al., 2012) y, por tanto la estrella estudiada puede haberse visto afectada por la transferencia de masa entre estrellas (Brott et al., 2012).

En este trabajo se estudiarán distintos mecanismos para tratar de ahondar más en el tema. En el apartado de *metodología* se explican los distintos pasos seguidos para el análisis de los datos y las estimaciones oportunas. Originalmente se contaba con una muestra de 847 estrellas, la cual fue reducida hasta 103 estrellas que cumplían una serie de criterios por los cuales estas estrellas se encuentran más cerca de la ZAMS y, además, tienen velocidades de rotación proyectadas, $v \sin i$, por debajo de los 60 $\mathrm{km\,s^{-1}}$. Los datos aquí usados han sido proporcionados por el grupo IACOB del IAC, cuyos espectros estelares han sido tomados por los telescopios NOT y MERCATOR en el Roque de los muchachos. También se han usado datos fotométricos proporcionados por el satélite TESS, dedicado a la buscada de exoplanetas, pero cuyas curvas de luz aportan también datos muy importantes en el ámbito de las estrellas masivas, ya que permiten obtener información asteroseismológica de las mismas.

En el apartado de *resultados y discusión* aparecen los resultados obtenidos tras llevar a cabo todos los análisis y cálculos necesarios. Se muestran los valores obtenidos para las velocidades de rotación proyectadas ($v \sin i$), la temperatura efectiva (T_{eff}), la gravedad superficial ($\log g$) y la abundancia de nitrógeno (log(N/H)+12) para cada una de las estrellas estudiadas. Usando las curvas de luz de TESS se puede medir la desviación típica del flujo (o magnitud) recibida durante 28 días de manera continuada, lo cual nos da una idea de la variabilidad de la estrella. También es posible la obtención de periodogramas a partir de dichas curvas de luz. Los periodogramas nos ayudan a interpretar las oscilaciones que tienen lugar en el interior de la estrellas, y con los valores aquí obtenidos se ha intentado buscar una correlación entre los distintos tipos de oscilaciones y la abundancia de nitrógeno. Cuatro tipos distintos de oscilaciones se tienen en cuenta: las oscilaciones de modos g, producidas en el núcleo como consecuencia de la gravedad; las oscilaciones de modo p que tienen lugar en la envoltura de la estrella y podrían ser la causa de la mezcla de materia entre las distintas capas estelares; las oscilaciones de modo híbrido que cuentan con oscilaciones tanto de modo p como de modo g; y las SLF (Stochastic Low Frequency), estrellas cuyos periodogramas muestran una gran abundancia de picos

en frecuencias cercanas a cero y que se ha postulado que están generadas por las llamadas "internal gravity waves" (Aerts & Rogers, 2015).

Hay un último apartado para las *conclusiones*. En general, no se han encontrado correlaciones claras durante el estudio. Uno de los mecanismos que podría estar afectando a las estrellas estudiadas son las oscilaciones de modo p, aunque hasta ahora se cree que son las oscilaciones de modo g las que podrían estar transfiriendo materia y energía del núcleo hacia las capas más externas, mientras que las de modo p solo estarían mezclando materia en los límites entre capas. Es decir, se ha observado, en algunos casos, lo contrario a lo que esperaríamos. De todas formas, las estrellas enriquecidas observadas que cuentan con oscilaciones de modo p, cuentan además con otros mecanismos que podrían estar provocando este aumento en nitrógeno en superficie. Sin embargo, las estrellas enriquecidas con oscilaciones en modo g no cuentan con otros mecanismos a parte para explicar el enriquecimiento.

La muestra inicial de estrellas se vio ampliamente reducida debido a la falta de observaciones para muchas de las estrellas. En un futuro nos podríamos beneficiar de nuevas observaciones espectroscópicas que nos permitan tener más información sobre los espectros de estrellas masivas. Cuanto más información de más estrellas, mayor será la estadística y mejores y más claros resultados se podrán obtener. Además, las curvas de luz usadas de TESS son aquelladas procesadas directamente por las pipelines estandar de la misión TESS, y muchas de las estrellas no han podido ser estudiadas ya que aunque contaban con datos de TESS, estos aún no habían sido extraídos de las Full Frame Images (FFI) y no han podido ser usados. Con el desarrollo de nuevas herramientas de análisis en el futuro se podrá trabajar con la totalidad de los datos ofrecidos por TESS, siendo estos tratados por nosotros mismo.

Abstract

In this MSc Thesis, different processes that take place inside massive OB-type stars will be studied to try to explain the reason why some of these stars have a nitrogen abundance in the surface higher than expected.

The work is divided into four parts, the first being an *introduction* to the field of massive stars and the background that has made it interesting to carry out this study today. Massive OB-type stars have been subject of research for decades since, due to their short life, they are a great source of information about the environment in which they are found. It was observed that some of these stars had a high abundance of nitrogen on the surface. An internal transport of matter from the stellar core to the surface was taking place, and materials obtained by burning H to He in the core by the so-called CNO cycle were being observed on the surface. High-mass stars have convective cores and radiative envelopes, so core material is not expected to reach the surface. The first theories seemed to indicate that this was happening due to mixing processes due to the high rotational velocities that these stars reach (Meynet & Maeder, 2000; Heger & Langer, 2000), but the appearance of new observations thanks to the VLT/FLAMES Survey of Massive Stars (P.I.S. Smartt) seemed to contradict what was assumed until then. The new observations found massive OB-type stars whose nitrogen abundance was high at the surface, but their projected rotational velocity, $v \sin i$, was too low (Hunter et al., 2008). Different studies were made to try to understand what was happening in this type of star with a low rotational velocity. Some mechanisms that could take place inside the star and that could produce this would be the presence of magnetic fields (Morel et al., 2008; Przybilla & Nieva, 2011), the oscillations that take place inside the star (Aerts et al., 2014). In addition, another thing to take into account is the binarity of the star studied (Brott et al., 2012).

In this work, different mechanisms will be studied to try to delve deeper into the subject. In the *methodology* section, the different steps followed to analyze the data and

the appropriate estimates are explained. Originally there was a sample of 847 stars, which was reduced to 103 stars that met a series of criteria for which these stars are closer to the ZAMS and, in addition, have projected rotational velocities, $v \sin i$, below 60 km s^{-1}. The data used here have been provided by the IACOB group of the IAC and the TESS satellite, mainly driven by the search of new exoplanets, but also providing very interesting information about variability of hundred thousands of stars which can be used to perform astrosesismic studies.

The results obtained after carrying out all the necessary analysis and calculations appear in the *results and discussion* section. The values obtained for the projected rotational velocities ($v \sin i$), the effective temperature ($T_{\rm eff}$), the srface gravity ($\log g$) and the nitrogen abundance (log(N/H)+12) are shown for each of the studied stars and we try to give some explanation based on other values also calculated. Using the TESS light curves we can get an idea of the variability of the star. It is also possible to obtain periodograms from these light curves. Periodograms help us interpret the oscillations that take place inside stars. Four different types of oscillations are taken into account: g-mode oscillations, produced in the stellar core as a consequence of gravity; the p-mode oscillations that take place in the envelope of the star and could be the cause of the mixing of matter between the different stellar layers; hybrid-mode oscillations that feature both p-mode and g-mode oscillations; and the SLF (Stochastic Low Frequency), stars whose periodograms show a great amount of peaks at frequencies close to zero, and that have been postulated to be generated by the so-called internal gravity waves (Aerts & Rogers, 2015).

There is a last section for the *conclusions*. In general, no clear correlations have been found during the study. One of the mechanisms that could be affecting to the stars are the p-mode oscillations, although it is believed that the g-mode oscillations are the ones that could be transferring matter and energy from the core to the outer layers, while the p- modes would only be mixing matter at the boundaries between layers.

List of Contents

1. Introduction

1.1. Massive stars

OB-type stars are massive stars in the blue part of their evolution. These stars are in the main sequence burning H in a convective core and, once they leave the main sequence, they evolve to red supergiants. Their mass is higher than 8-10 $M_\odot$ and they have a short lifetime of $\backsim 10^6$-10^7 years. Only some of these stars are formed compared to the low mass stars, and are one of the most luminous objects in the Universe. They emit strong UV radiation that ionizes the interstellar medium and creates a so-called HII region. Since they have short lifes, they do not have time to move far from the original place where they were formed, therefore they show the present-day chemical composition of the zone where they are. Thanks to it, these stars can be used to study abundance gradients in nearby galaxies using atmosphere models developed in the last years. Still, there are some mechanism that can be altering the surface chemical composition in these stars and that have to be carefully studied: stellar mass-loss, rotational mixing contaminating surface abundances or mass transfer in binary systems.

NLTE atmosphere models allows us to obtain both stellar parameters and surface abundances with great precision. Equivalent width of metal lines depends on $T_{\rm eff}$ and $\log g$ of the star and are related to chemical abundances. With a good estimation of these parameters a good analysis can be done to obtain the most accurate abundances.

Massive OB stars in the main sequence burn H producing He via CNO cycle in a convective core. These produced elements are not expected to reach the surface since the convective core is surrounded by a radiative envelope. The existence of CNO-cycled matter–resulting from the burning of H into He in the convective core of massive stars–reaching the stellar surface can be empirically investigated by determining the surface abundance of N via quantitative spectroscopy. This work will focus in N abundances estimated for a set of OB stars and the mechanism that could be producing this such

as rotational and pulsational mixing effects, magnetic field effects or binarity. Individual objects showing higher N abundance than expected will be discussed considering their characteristics to try to find an explanation that is yet unknown.

1.2. State of the art

Massive star evolution has been long studied by different astrophysics for years. A characteristic He and N enrichment was observed in many of these stars (Walborn, 1976; Walborn, 1988; Langer, 1992; Herrero et al., 1992) but it was in 2000 when rotational mixing started to be considered in massive star evolution by Meynet & Maeder (2000) and Heger & Langer (2000). Theories showed that nitrogen enrichment could be produced by high rotational velocities in the stars that were transferring hydrogen-burning products from the core to the surface due to rotational mixing. This also would be a good way to determine if a star is a fast rotator just considering their N abundance in the surface. But this idea changed when VLT/FLAMES survey (Evans et al., 2005) was released, and a new amount of stellar parameters and nitrogen measurements were available for massive main sequence stars in a wide range of projected rotational velocities. A high number of fast rotators among B-type stars (i.e. main sequence stars with masses in the range 8-15 $M_{\odot}$) with low nitrogen abundance and slow rotators with high nitrogen abundance were found in the Large Magellanic Cloud by Hunter et al. (2008), which means that rotational mixing might not be the main origin of this enrichment and other mechanism must be taken into count (Brott et al., 2012). Rivero et al. (2012) extended the previous studies to main sequence stars with higher masses by estimating nitrogen abundance from a sample of O-type stars in the LMC using the NLTE stellar atmosphere code *FASTWIND* (Puls et al., 2005), and found that the same as in B-type stars was happening.

Observational data also shows that stars with a detected magnetic field might have a higher incidence of chemical peculiarities (Morel et al., 2008) and this could be causing than some slow rotating massive stars might be nitrogen enriched due to the presence of a magnetic field. Stars with an expected nitrogen abundance has not been observed to be magnetic, except for some particular cases. With more data available, a correlation between mixing signatures and the presence of magnetic fields was found by Przybilla & Nieva (2011) which, in low rotational stars, might imply that magnetic breaking is highly efficient for spin-down in some massive stars. The presence of magnetic field could be

slowing down stars that used to be fast rotators.

The small sample of studied stars has led to think that this enriched stars might be rapid rotators viewed nearly pole-on (Brott et al., 2012), so sin$i$ makes the $v$sin$i$ seem smaller than it actually is. To improve the studies we need precise measurements of the inclination angle i between the rotational axis and the line-of-sight, and also of $v$sin$i$ (Aerts et al., 2014). This two values (i, $v$sin$i$) are known for very few stars and improving the observations would help in this work. Comparisons of results obtained by the VLT-FLAMES survey of massive stars and population synthesis simulations found that the number of observed stars with $v$sin$i$ between 40-80 km/s and high nitrogen abundances was consistent with these stars being rapid rotators (Dufton et al., 2018, 2020). However, the number of stars with $v$sin$i$<40 km/s and large nitrogen abundances was too high compare with simulations. A possible explanation for this is that magnetic effects may be playing an important role although the comparison is difficult.

The possible role of binary stars in nitrogen enrichment (Brott et al., 2012) shows that slowly rotating nitrogen-enriched stars are unlikely to be produced via mass transfer and tidal spin-down in close binary systems.

An alternative explication for this could be the presence of pulsational mixing in the stellar interior. Aerts et al. (2014) investigated possible correlations between N abundances and difference stellar properties, including the frequency and amplitude of dominant p and g modes, for a sample of 64 galactic OB stars. These stars has a $v$sin$i$ < 100 km/s and nitrogen abundance between 7 and 9 dex, and neither rotational velocity, frequency nor amplitude show a correlation with N abundance. However, heat-driven oscillation mode frequencies seems to be a more suitable predictor for mixing comparing to magnetic field or rotation.

The CNO-cycled matter mixing might be occurring in an early hydrogen burning phase for a considerable fraction of massive stars and this might be produced by other mechanism that does not include rotational mixing (Aerts et al., 2014; Rivero et al., 2012).

1.3. Asteroseismology

Processes taking place in the internal layers of a star can be studied thanks to seismology, since a star works as a resonant cavity with two possible propagation modes (Aerts et al., 2010):

- *Acoustic* mode (or p-mode). The restoring force is the pressure and are mainly located in the surface of the star.
- *Gravity* mode (or g-mode). The restoring force is buoyancy and propagate to the inner part of the star, even reaching the boundary of the stellar core.
- *Hybrid mode*. Both acoustic and gravity modes appear in the stellar interior. These modes have information on the stellar interior and reach the surface with larger amplitudes than g-modes. Their detection is possible in evolved stars because of the coupling between the g-mode and p-mode cavity.

As ilustration of hybrid modes taking place in the interior of stars, Bedding et al. (2011) showed that these modes are a precise tool to differentiate red supergiants that are burning hydrogen from others that are burning helium in the core.

In this work we will also consider stars with Stochastic Low Frequency (SLF). The periodograms of these stars show a lot of peaks getting bigger at frequencies close to zero.

The pulsations modes are studied in the Fourier domain. In this work we will use the Lomb-Scargle Fourier Transform to get periodograms of the star as a function of a power spectrum. It is possible to measure the frequency of the maximum power and with it we can obtain information about the oscillation modes in the star and the possible mixing mechanism taking place in the interior (Beck et al., 2012).

1.4. Motivation

The main goal of this work is to study different mechanism occurring in OB-type massive stars and, with them, try to explain the presence of CNO-cycled matter in the surface on this star, considering a sample with low rotational velocities. This will be done by implementing already existing analysis techniques to estimate nitrogen abundance of a sample of stars. Our quantitative spectroscopic analyses will be based on a vast grid of synthetic spectra computed with the stellar atmosphere code *FASTWIND* (Puls et al., 2005).

This work also benefit from the availability of light curves of exquisite quality delivered by the TESS mision. We will extend the previous work done by Aerts et al. (2014) to a bigger star sample. In this case, new observational data will be used to get periodograms

and to study the star from an asteroseismic perspective, considering which role play the three existing modes of oscillation, their frequency and amplitudes in the nitrogen enrichment in the surface of the studied stars.

Another possibility that will be considered and studied here is the binarity of the stars. Using spectroscopic data we will check if any of the stars is part of a binary system since, in this case, the nitrogen abundance discrepancies may be caused by a mass transfer from a binary sister to the surface of our star.

The relation between rotational velocity and nitrogen abundance has been long studied, but the other explained mechanism are just starting to be considered to play a role in this field. With this work we want to perform an extended analysis of all of these mechanism and set a starting point to expand this study to larger samples of stars to have a better statistics. This way, considering all the possible processes in stellar interiors, an explanation to the existence of stellar surfaces in B-type slow rotators with enriched N abundances might be found soon.

2. Methods

2.1. Observations

The observational data considered in the work comes from the IACOB spectroscopic database (Simón-Díaz et al., 2020) and the TESS mission (Ricker et al., 2014).

2.1.1. Stellar spectra

Spectroscopic data from the studied stars has been taken from the IACOB spectroscopic database [1] (latest described in Simón-Díaz et al., 2020).

Considered spectra were obtained with three different instruments (Holgado et al., 2018):

- The **FIES** spectrograph attached to 2.56m-Nordic Optical Telescope (NOT) at Roque de Los Muchachos Observatory. This instrument has a resolving power of 46000 and 25000 and works in a wavelength range 3750-7250 Å.
- The **HERMES** spectrograph attached to 1.2m-MERCATOR Telescope at Roque de Los Muchachos Observatory with a resolving power of 85000 and a wavelength range 3700-9000 Å.
- The **FEROS** spectrograph attached to ESO/MPG-2.2m Telescope at La Silla Observatory. This instrument has a resolving power of 46000 and a wavelength range 3530-9210 Å.

All of these spectra are normalized and corrected from heliocentric velocity. Despite the difference in resolving power, the three instruments are very similar and their Signal to Noise Ratio (SNR) is above 100 in most of the considered spectra. A resolving power

[1] http://research.iac.es/proyecto/iacob/pages/en/iacob-spectroscopic-database.php

higher than 25000 is more than enough to analysis the parameters that we want to study in this work.

2.1.2. TESS light curves

This work also makes use of photometric data to study stellar brightness and variability. These photometric data has been taken from TESS mission database[2] (Ricker et al., 2014).

The Transiting Exoplanet Survey Satellite (TESS) began its observations in 2018 and its main goal is to detect Earth-sized planets orbiting bright stars (Ricker et al., 2014). It has four lenses with a combined field of view of 24ºX96º, dividing the sky in 26 overlaping sectors (13 in each hemisphere) that are observed for 27.4 days (two satellite orbits). TESS sends a series of Full Frame Image (FFI) with an effective exposure time of 30 minutes, and also monitors 200000 pre-selected stars with a 2 minutes cadence. It has a spatial resolution of 21 arcsec/pixel.

The mission is currently observing sector 52. Some of the sectors (specially those pointing to the galactic disc) have a large amount of OB type stars for which IACOB survey have also accessible spectra (see, e.g., Burssens et al., 2020). This means that our studied stars have been also observed by TESS and thus, their photometric data is accessible and ready to be used. We are interested in the study of light curves (LC) provided by TESS. These are already available in calibrated form as Simple Aperture Photometry (SAP). Some of the stars has been observed by TESS more than once, so more of one LC can be studied.

With this data is not only possible to study the variability of the star by their LC, but also the type pulsations taking place in the stellar interior by analyzing their periodograms (see Section 2.5.1). However, a word of caution; since every pixel has a size of $\backsim$0.3 arcmin we have to take care of the information provided by TESS. Stars occupy around 6-8 pixels in every axes as shown in Fig. 2.1, which give a size of $\backsim$2 arcmin. This is a big region for one single star, and we have to consider that some other stars brightness could be affecting the light curve given by TESS. This is why a study based on possible "contaminants" in the stars have to be done. To do this we can make use of Gaia Archive and the Washington Data Survey to get information about this star and other stars that could be in a region

[2] https://tess.mit.edu/

smaller than 2 arcmin from our star. If any other star has been observed 2 arcmin or less from the studied stars, we will consider that this star has comtaminants and thus its light curve results will have to be studied carefully.

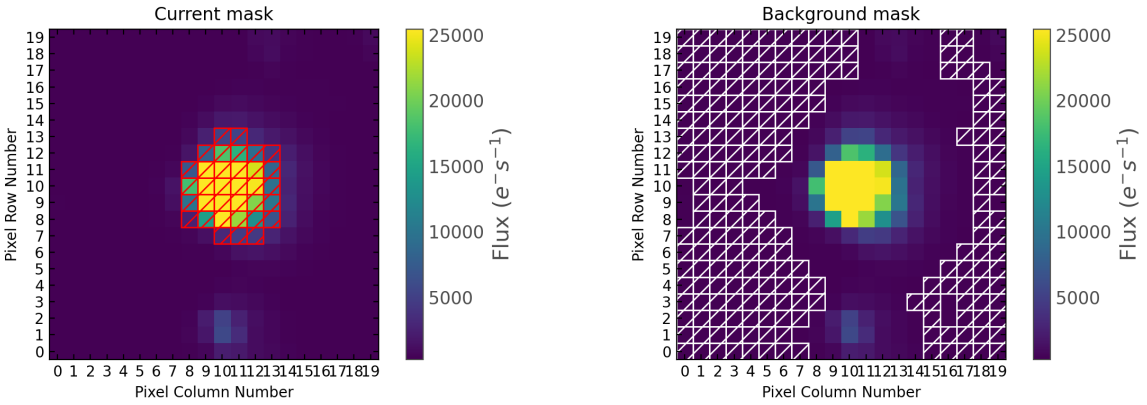

Figure 2.1.: Portion of a FFI-TESS CCD showing the flux that gets into every pixel and the mask used for star HD35337.

2.2. Analysis Tools

This work uses the following spectroscopic analysis tools (most of them developed in the framework of the IACOB project):

- The *iacob-broad* tool (Simón-Díaz & Herrero, 2014) is an IDL package used to estimate $v \sin i$and $v_{\rm mac}$ and that combines a Fourier transform (FT) + Goodness of fit (GOF) analysis strategy to provide several solutions for the pair of line-broadening parameters.
- The *ew-global* tool, also implemented in IDL by S. Simón-Díaz, allows to measure equivalent widths (EW) from spectral lines of a desire chemical element.
- The *si234-analisis* and *spec-fit* IDL tools allows the estimation of $T_{\rm eff}$ and $\log g$ values by simulating stellar conditions models and fitting them to our data. Both packages make use of an extense grid of synthetic spectra computed with the stellar atmosphere code FASTWIND (see below).
- The *superab* tool allows to estimate the nitrogen abundance of stars with a given set of $T_{\rm eff}$ and $\log g$ values.

- *FASTWIND* (Puls et al., 2005) is a stellar atmosphere/line formation code designed for optical and IR spectroscopic analysis of stars with spectral type from A to O. This code considers NLTE conditions, spherical symmetry, mass-loss and stellar winds.
- *Atomic Line List* from University of Kentucky [3]. Compiles 1.72 million allowed and forbidden atomic transitions in the range from 0.5 Å to 1000 μm, taken from NIST Atomic Spectra Database and other studies.
- *Mathematica* and *pyhton* codes specially developed for the aim of this study:
  - Manage IDL tools results and plotting the corresponding figures.
  - Analysis of photometric variability and light curves.
  - Obtaining and study of Periodograms.
  - Spectral analysis of binarity.

2.3. Sample Selection

In order to study the role that nitrogen abundance plays in massive OB stars, we need to consider an optimal selection of stars whose properties are suitable for this case of study.

We start considering an initial sample of 847 stars (see Fig. 2.2) for which the IACOB project had obtained a preliminary estimation of the effective temperature ($T_{\rm eff}$), surface gravity ($\log g$) and projected rotational velocities ($v \sin i$). From this initial sample of stars available only those that are in the main sequence (MS), especially those closer to the zero age main sequence (ZAMS), will be considered in this study. This MS stars selection can be done considering the gravity ($\log g$) of the giving stars. The selection of stars has been done taking only the stars in a $\log g$ range of 3.7-4.3 dex, since these are the closest stars to the ZAMS.

Another limit considered in the sample is related with the stellar mass. We have selected stars with mass $\gtrsim$9 $M_\odot$.

This preinitial sample includes stars with a broad range of $v \sin i$ values (see Fig. 2.2). In this study we just want to consider those massive stars that are slow rotators, that

[3] https://www.pa.uky.edu/∽peter/newpage/index.html

means that have a low $v \sin i$. Nitrogen enrichment in slow rotators has not been explained yet and the aim of this study is to try to find an explanation. Consequently, from these stars it has been considered for this work only those stars with a $v \sin i$ below 60 km/s.

This concludes with an star sample of 103 stars. But in order to study the chemical abundances of the stars we need to work with stars that have NII diagnostic lines, and this leds us to choose stars with mass below 25 $M_\odot$ (see Fig. 2.5). The sample was reduced to 60 stars in a mass range from 9 $M_\odot$ to 25 $M_\odot$ and a good Signal to Noise ratio(SNR). From these 60 stars, the nitrogen abundance estimation has been done with 51 of them, while for 9 of the stars it was not possible to get an abundance estimation. The position of each star in the Kiel Diagram is shown in Fig. 2.2 together with the stellar evolutionary tracks from the non-rotating stellar evolution models by Ekström et al. (2012), depicted for reference. Figure 2.2 is complemented with Fig. 2.3, which shows a complete distribution of stars available for each $v \sin i$. The histogram in the right in 2.3 considers the 103 stars with $v \sin i$<60 km s^{-1}, where only the black marked stars will be studied.

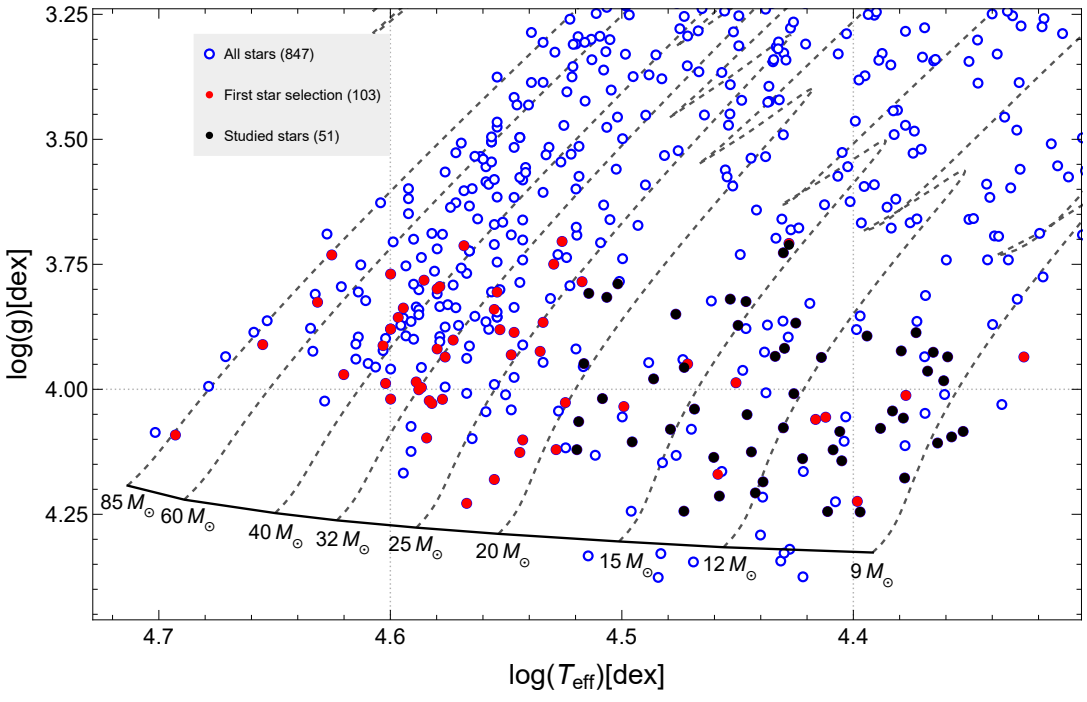

Figure 2.2.: Kiel diagram for the whole sample of stars considered in this study representing log(g) at Y axes. The preliminary selected stars are marked in red. The final studied stars are marked in black.

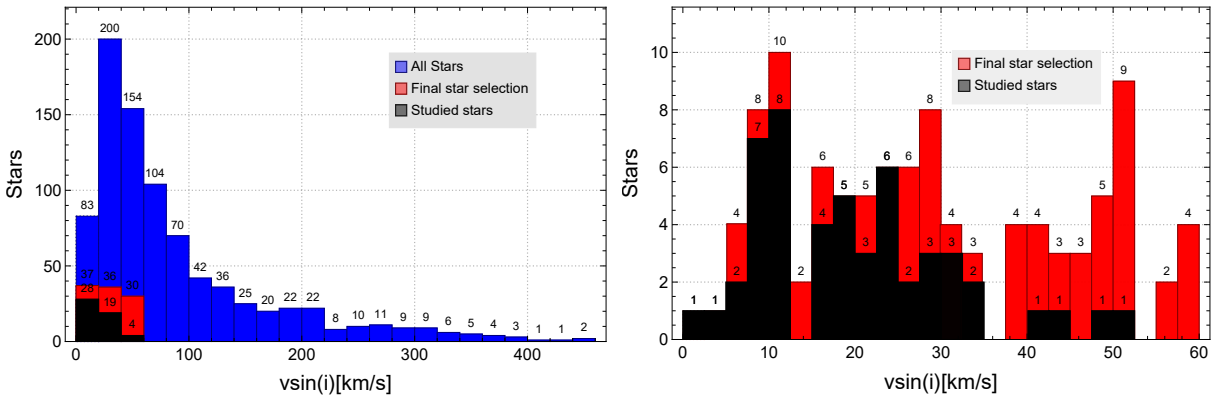

Figure 2.3.: Histogram showing the total sample of 847 stars (left) and a zoom into the 103 stars selected with rotational velocities lower than 60 km s^{-1}(right).

2.4. Quantitative spectroscopic analyses

This part explains the quantitative spectroscopic analyses used to get information about the projected rotational velocities, $v \sin i$, the effective temperature, $T_{\rm eff}$, and the gravity, $\log g$, of the stars. With this information we will be able to estimate the values of nitrogen abundance in the stellar surface. This is made thanks to line spectroscopy by measuring equivalent widths of elements of interest and by simulating stellar conditions using different available grids.

2.4.1. Projected rotational velocity

The first thing that needs to be done before starting with spectral line analysis is to measure the $v \sin i$ values since we want to prove if $v \sin i$ and nitrogen abundance are related and they will be needed later in the estimation of equivalent widths.

In this work $v \sin i$ has been calculated using the *iacob_broad* IDL package. This package uses SiIII λ4452 Å line to get the best fit and do a Fourier Transform whose first zero value give us the projected rotatonal velocity corresponding to the studied Si line. The line fitting is done by using Goodness of Fit (GOF) methodology. When measuring the $v \sin i$using FWHM methods we need to be careful in this case in which we study OB massive stars especially when applied to HeI lines. The Fourier Transform method has been shown to be a better and more precise way to estimate the $v \sin i$by also separating

the rotational effects from other broadening effects that occurs in stellar spectra as checked by Simón-Díaz & Herrero (2007, 2014).

This combination of Goodness of Fit (GOF) + Fourier Transform measures not only the $v\sin i$ but also the macroturbulent effects in the broadening of the spectral lines (Simón-Díaz & Herrero, 2014). This give us better rotational velocity results.

Figure 2.4 shows the rotational velocities measured with the GOF+FT method for this work and compare them with the preliminar $v \sin i$ estimations that I had accesible at the beggining of this work (see Section 2.3). It can be appreciated that the velocity values used in this work are quite similar to those obtained by my supervisor, so it is considered that they are optimal to continue with the line spectroscopy study.

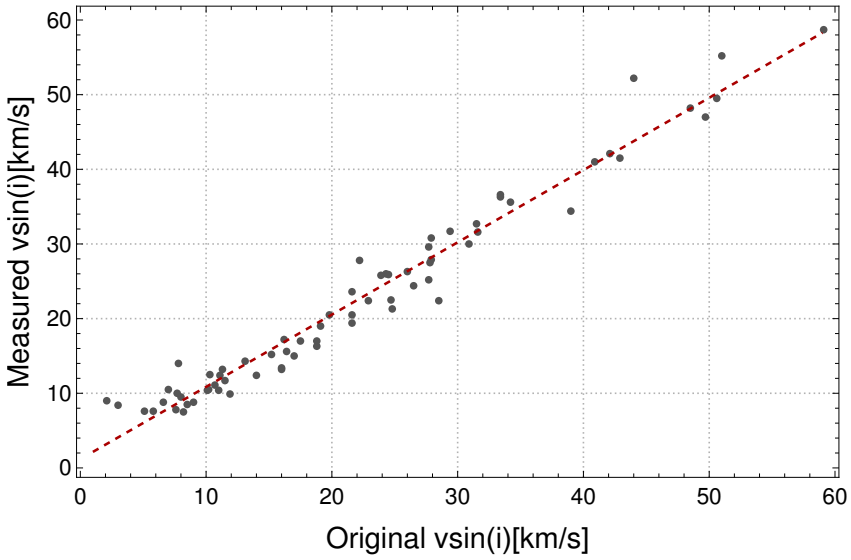

Figure 2.4.: Comparison between the measured $v \sin i$ as part of the quantitative spectroscopic analysis performed in this work with the preliminar values previously obtained by my supervisor.

2.4.2. N and Si equivalent widths

Once the rotational velocities are obtained, the next step is to measure the equivalent widths of some spectral lines of interest. All silicon and nitrogen lines appearing in the stellar spectra have been measure using the IDL package *auto_ew*. This one uses the executable *ew_global* to fit the spectral lines of the desired elements, considering the radial velocity previously determined, and to give the equivalent width values and the

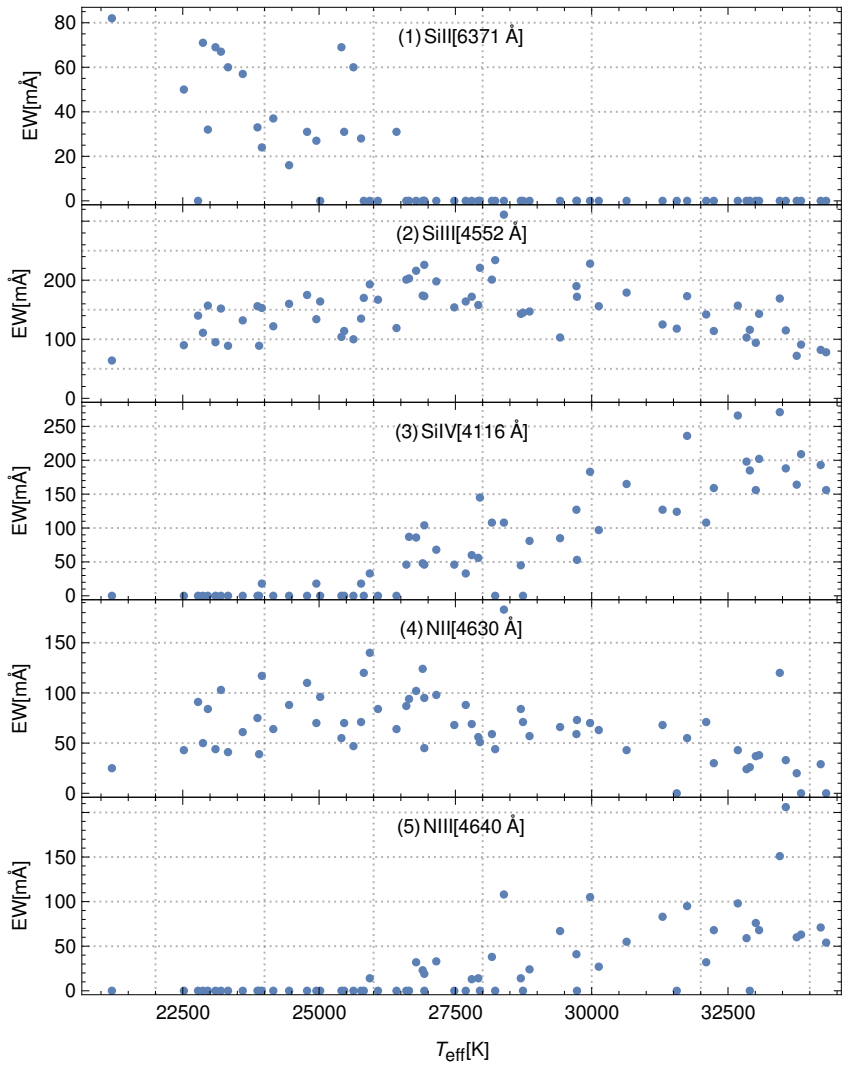

Figure 2.5.: Equivalent width estimates for 5 different diagnostic lines of Si and N for the whole sample of stars considered in this work.

fitting plot. Using the obtained plot we can verify if any of the lines are blended or even if any of them has been incorrectly fitted.

With all N and Si spectral lines measured the next step is to considered those lines needed in this work and select them. Using a *mathematica* code, all the equivalent widths determined with *ew_global* have been studied and plotted and what has been seen is that there are four main Si lines of interest in for this work. This correspond to Si II λ4128 Å, Si II λ6371 Å, Si III λ4552 Å and Si IV λ4116 Å. In Fig. 2.5 are shown the EW and $T_{\rm eff}$ for every star. Those stars with $T_{\rm eff}$ lower than $\backsim$ 25000 K has the Si II λ6371 Å line

(also Si II λ4128 Å) meanwhile those stars with higher $T_{\rm eff}$ than $\backsim$ 25000 K has the Si IV λ4116 Å line, and all of them has the Si III λ4552 Å. Different EW ratios have been calculated to be used in the determination of $T_{\rm eff}$ and $\log g$ later. For lower $T_{\rm eff}$ the ratio SiII/SiIII is used to constrain the effective temperature, but two different SiII lines were measured so we need to check which one give us better results. In this case we study the ratios Si II λ4128 Å/Si III λ4552 Å and Si II λ6371 Å/Si III λ4552 Å. For higher $T_{\rm eff}$ the ratio that will be used is Si IV λ4116 Å/Si III λ4552 Å. There are some stars around 25000 K that have the four Si lines in their spectra, so the three ratios were done.

In case of nitrogen, a lot of lines were measured for each star. These lines are used to estimate the abundance and, depending of every star, the selection of the lines has to be done for every star one by one. Figure 2.5 shows the EW for the different studied stars in two case (N II λ4630 Å and N III λ4640 Å) as an example: NII lines are existing in most of the stars, while NIII only appears in some the hottest stars.

Another value that *ew_global* gives is the Signal to Noise Ratio (SNR). When having a big sample of stars, it is useful to select the stars with the best SNR since they will have more precise results. In this study only 60 stars were studied after considering its SNR, but the N abundances was measured only 51 of them.

2.4.3. Effective temperature and surface gravity

Knowing the EWs of the various accessible Si diagnostic lines and the corresponding SiIV/SiIII and/or SiII/SiIII ratios of EWs calculated in the previous section, the $T_{\rm eff}$ and $\log g$ can be estimated more accurately for our stars. These $T_{\rm eff}$ and $\log g$ values were measured using different techniques. To get the best nitrogen abundance results we need to use the best $T_{\rm eff}$ and $\log g$ values possibly achievable.

First, a set of new values for the $T_{\rm eff}$ and $\log g$ are obtained and, studying Balmer lines broadening, it is possible to decide which is the best $T_{\rm eff}$-$\log g$ combination from the obtained range of values. The IDL package *si234_analisis* allows to simulate different stellar conditions starting from the Si ratio and its numerical value, the stellar wind and the microturbulence of the star. This package uses a set of synthetic spectra computed with the stellar atmosphere code *FASTWIND* (Puls et al., 2005; Simón-Díaz et al., 2011) for massive stars.

With another IDL package, *spec_fit*, it is possible to measure the gravity of the star

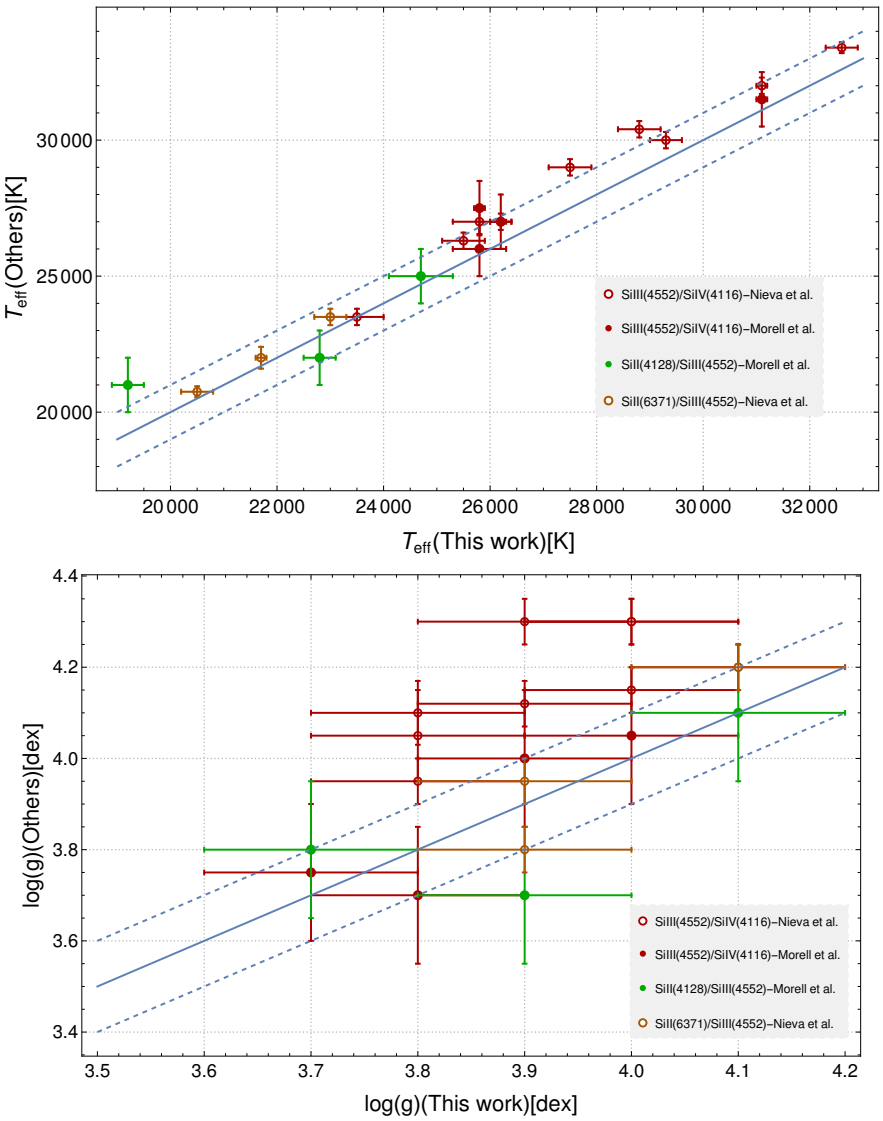

Figure 2.6.: Comparison between the measured log(g) and temperatures with those obtained by Morel et al. (2008) and Nieva & Przybilla (2012).

by fitting a *FASTWIND* model in Balmer Hydrogen lines. This package uses different given grids that vary according to $T_{\rm eff}$, $\log g$ and stellar wind and fits these models to hydrogen absorption lines (Hα, Hβ, Hγ and Hδ). We can consider the $T_{\rm eff}$-$\log g$ values simulated with *si234_analisis* and see which pair best fits these Balmer lines. This way it is possible to obtain a good $\log g$ value that will be used later in the estimation of nitrogen abundance. Once we have the $\log g$, the $T_{\rm eff}$ is the one obtained before using *si234_analisis* corresponding to this $\log g$. As we have mentioned in sec-

tion 2.4.2, stars with low temperatures has two different SiII diagnostic lines to compute the temperature together with Si III λ4552 Å and, as it was already seen in Simón-Díaz (2010), the ratio Si II λ6371 Å/Si III λ4552 Å give us better results than the ratio Si II λ4128 Å/Si III λ4552 Å. In this work Si II λ6371 Å/Si III λ4552 Å will be used to make the $T_{\rm eff}$ estimations.

To prove our estimated values of $T_{\rm eff}$ and $\log g$ are correct, a comparison with the literature was made. First Morel et al. (2008) and later Nieva & Przybilla (2012) studied some of the stars also studied in this work. We use this 15 stars in common to check if our measurements are being done correctly. Table 2.1 shows the $T_{\rm eff}$ and $\log g$ for these stars in this work and also these other studies. Figure 2.6 shows the comparison between the values obtained in this work and those obtained by Nieva & Przybilla (2012) and Morel et al. (2008). We can see that Morel et al. (2008) used Si II λ4128 Å to get the values of low $T_{\rm eff}$ stars, while Nieva & Przybilla (2012) used Si II λ6371 Å. Considering the case of star *HD3360* we can appreciate this: our measurements made with Si II λ4128 Å are similar to those from Morel et al. (2008), while the measurements for this same star but using Si II λ6371 Å is more similar to those from Nieva & Przybilla (2012). In these cases where we have to values depending on the SiII line used, this work will consider those corresponding to Si II λ6371 Å since it is more reliable.

2.4.4. Nitrogen abundances

Finally, after all the previous analyses, it is possible to obtain estimates of the nitrogen abundance of any 60 stars in our sample. To this aim, we use the IDL package *Abun_analisis*, more specifically the executable *superab* that allows to study elements abundances and their microturbulence using the already known values of $T_{\rm eff}$, $\log g$ and the EW measurements. It can do this by using a file with EW calculated with FASTWIND and the EW measured in our spectra. Each of the stars has to be studied separately, and the final set of optimal NII diagnostic lines considered in the analysis has to be inspected carefully to identify lines which could be affected by blends or had incorrect atomic data. The problematic lines must be excluded from the abundance analysis.

When the N lines are chosen the analysis is done for a $T_{\rm eff}$ interval of $\pm$ 500 K, this way the uncertainties due to temperature differences can be considered. Also, this kind of analysis gives a range of abundance values for a given range of estimated microturbulences($\xi_{\rm t}$).

Table 2.1.: Comparison between our results and the results obtained by Nieva & Przybilla (2012) and Morel et al. (2008) for each star. Second column shows the $T_{\rm eff}$, $\log g$ and N abundance results obtained in this work, considering the three possible Si ratios which are shown in the Table as: Si IV λ4116 Å/Si III λ4552 Å (A), Si II λ4128 Å/Si III λ4552 Å (B), Si II λ6371 Å/Si III λ4552 Å (C). The uncertainties for $\log g$ in this work are 0.1 dex in all the stars. In third column we show $T_{\rm eff}$, $\log g$ and N abundance results obtained by Morel et al. (2008) and in fourth column are the results from Nieva & Przybilla (2012). The uncertainties of the values appear between brackets.

star	TFM ALEX									MOREL			NIEVA		
	$T_{\rm eff}$			log(g)			Log(N/H)+12			$T_{\rm eff}$	log(g)	log(N/H)+12	$T_{\rm eff}$	log(g)	log(N/H)+12
	A	B	C	A	B	C	A	B	C						
HD85953	-	19.2 (0.3)	18.8 (0.3)	-	3.7	3.6	-	7.67 (0.18)	7.70 (0.18)	21.0 (1)	3.80 (0.15)	7.66 (0.20)	-	-	-
HD3360	-	22.8 (0.3)	20.5 (0.3)	-	3.9	3.9	-	8.14 (0.06)	8.37 (0.14)	22.0 (1)	3.70 (0.15)	7.97 (0.11)	20.75 (0.2)	3.80 (0.05)	8.23 (0.07)
H157056	-	24.7 (0.6)	22.7 (0.9)	-	4.1	4	-	7.75 (0.06)	7.86 (0.08)	25.0 (1)	4.10 (0.15)	7.78 (0.10)	-	-	-
HD886	-	23.3 (0.2)	21.7 (0.1)	-	3.9	3.9	-	7.53 (0.07)	7.77 (0.09)	-	-	-	22.00 (0.4)	3.95 (0.05)	7.76 (0.07)
HD35299	23.5 (0.5)	24.4 (0.5)	23.0 (0.3)	4.1	4.1	4.1	7.76 (0.07)	7.72 (0.06)	7.80 (0.06)	-	-	-	23.50 (0.3)	4.20 (0.05)	7.82 (0.08)
H205021	25.8 (0.5)	-	-	3.8	-	-	7.98 (0.08)	-	-	26.0 (1)	3.70 (0.15)	7.91 (0.13)	27.00 (0.45)	3.95 (0.05)	8.11 (0.11)
HD36591	26.2 (0.2)	-	-	3.9	-	-	7.72 (0.08)	-	-	27.0 (1)	4.00 (0.15)	7.66 (0.12)	27.00 (0.3)	4.12 (0.05)	7.75 (0.09)
HD36960	27.5 (0.4)	-	-	3.8	-	-	7.53 (0.12)	-	-	-	-	-	29.00 (0.3)	4.10 (0.07)	7.72 (0.11)
HD34816	28.8 (0.4)	-	-	3.9	-	-	7.55 (0.16)	-	-	-	-	-	30.40 (0.3)	4.30 (0.05)	7.81 (0.15)
HD36822	29.3 (0.3)	-	-	3.8	-	-	7.90 (0.16)	-	-	-	-	-	30.00 (0.3)	4.05 (0.1)	7.92 (0.10)
H149438	31.1 (0.1)	-	-	4.0	-	-	8.10 (0.08)	-	-	31.5 (1)	4.05 0.15	8.15 (0.20)	32.00 (0.3)	4.30 (0.05)	8.16 (0.12)
HD46328	25.8 (0.1)	-	-	3.7	-	-	8.02 (0.09)	-	-	27.5 (1)	3.75 (0.15)	8.00 (0.09)	-	-	-
HD61068	25.5 (0.4)	-	-	4.0	-	-	7.96 (0.11)	-	-	-	-	-	26.30 (0.3)	4.15 (0.05)	8.00 (0.12)
HD36512	32.6 (0.3)	-	-	4.0	-	-	7.69 (0.27)	-	-	-	-	-	33.40 (0.2)	4.30 (0.05)	7.79 (0.11)

The uncertainties induced by this $\xi_{\rm t}$ range are also considered in the final result. Finally, there is another uncertainty that appears due to the dispersion of the different N lines that are studied. The N abundances are given in dex units as log(N/H)+12. Table 2.1 shows the comparison between log(N/H)+12 measured here and those from the literature. In stars where both Si II λ4128 Å and Si II λ6371 Å are available this work has finally settle for those values obtained with the analysis of Si II λ6371 Å such in Nieva & Przybilla (2012). Figure 2.7 shows the comparison of N abundances for those stars in common with Morel et al. (2008) and Nieva & Przybilla (2012). Once the analysis is verified to work correctly, it is possible to continue studying the rest of the star sample.

All the final results obtained with this analysis are in table 3.1. From the 60 inicial star sample, it was possible to estimate the log(N/H)+12 for 51 of them. The other 9 stars gave some problems in the determination due to their lack of NII/NIII lines.

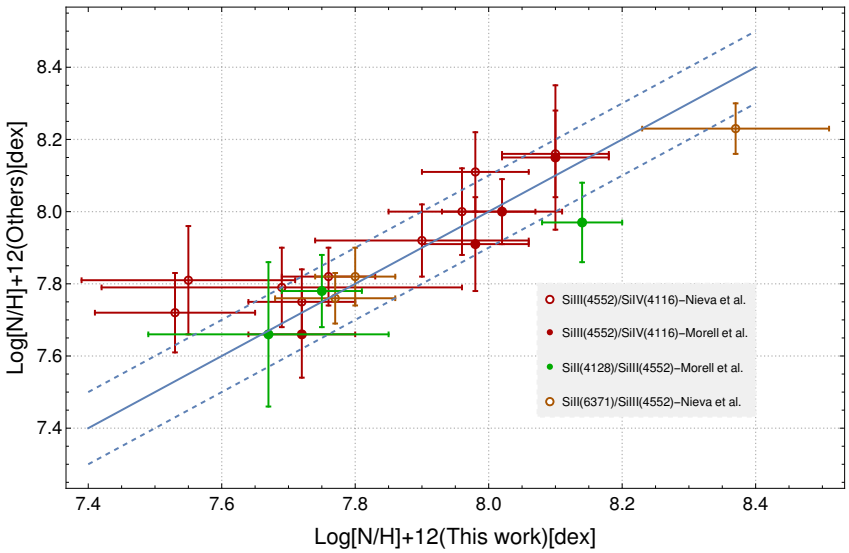

Figure 2.7.: Comparison between the measured nitrogen abundances and those obtained by Morel et al. (2008) and Nieva & Przybilla (2012).

2.5. Variability, oscillations and binarity of stars

This study aims to prove different mechanism which has been proposed to be able to drive chemical mixing in massive OB stars. Apart from the rotational mixing, which in this case the star selected are slow rotators, other mechanism that could raise N abundance in the stellar surface are pulsations taking place in the inner parts of the star (Aerts et al., 2014; Burssens et al., 2020), or could be that what it seems to be a single star is actually a binary star and the N abundance could be explained by mass transfer between the stars.

2.5.1. TESS light curves analysis: variability and oscillations

Using TESS light curves is possible to get accurate measurements of the amplitude of photometric variability and pulsation frequency of the stars. A total number of 36 of the studied stars has been observed with TESS and their light curves have been processed by TESS Mission. This gives a light curves enough to study if there could be any relation with the N abundance.

Using a *mathematica* code it was possible to study these light curves and to get information about both the amplitude of variability and the dominant pulsation frequency

of each star. This can be achieved by doing a Lomb-Scargle Periodogram (Lomb, 1976; Scargle, 1982) for the given light curves. The LS-Periodogram has been used since way long to characterize the periodicity in time-series data like the one that TESS provide, by doing a Fourier-like Transform power spectrum (VanderPlas, 2018). The LS-Periodogram equation in this work (derived from Lichtblau, 2006) is the following

$$P_{LS}(\omega) = \frac{\sqrt{\left|\sum(flux-\mu)e^{-i(\omega t-\tau(\omega))}\right|^2}}{2\sigma\sum\left|(e^{-i(\omega t-\tau(\omega))})^2\right|} \tag{2.1}$$

$$\tau(\omega) = Arctan\left(\frac{\sum 2\cdot sin(\omega t)}{\sum 2\cdot sin(\omega t)}\right) \tag{2.2}$$

For a given flux, this algorithm finds a numerical solution to plot the power spectrum as a function of the frequency. With this periodogram it is possible to measure the different peaks where the puls occur and the frequency of this puls, allowing us to know what kind of puls they are and what kind of internal processes might be taking place in the stellar interior. In this work, all the periodograms have been normalized to the amplitude of the maximum peak and thus the amplitude of the other frequency peaks are expressed as percentage of the maximum. An example of these measurements is shown in Fig. 2.8 with the light curve for HD61068 and its periodogram with the frequency of its two peaks. This star appears to have p-mode pulsation since the main peak frequency is located at 6 cycles/day. The periododogram of this star was also studied by Burssens et al. (2020) and the analysis are compatible, so the rest of the stars has been studied using the same algorithm. Figures 2.9 show the periodograms for the different types of pulsators that have been identified in our sample (see also Section 1.3).

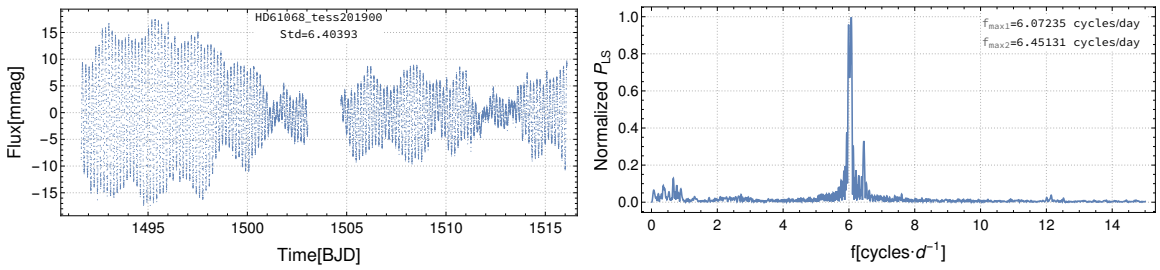

Figure 2.8.: TESS light curve and Lomb-Scargle periodogram for HD61068.

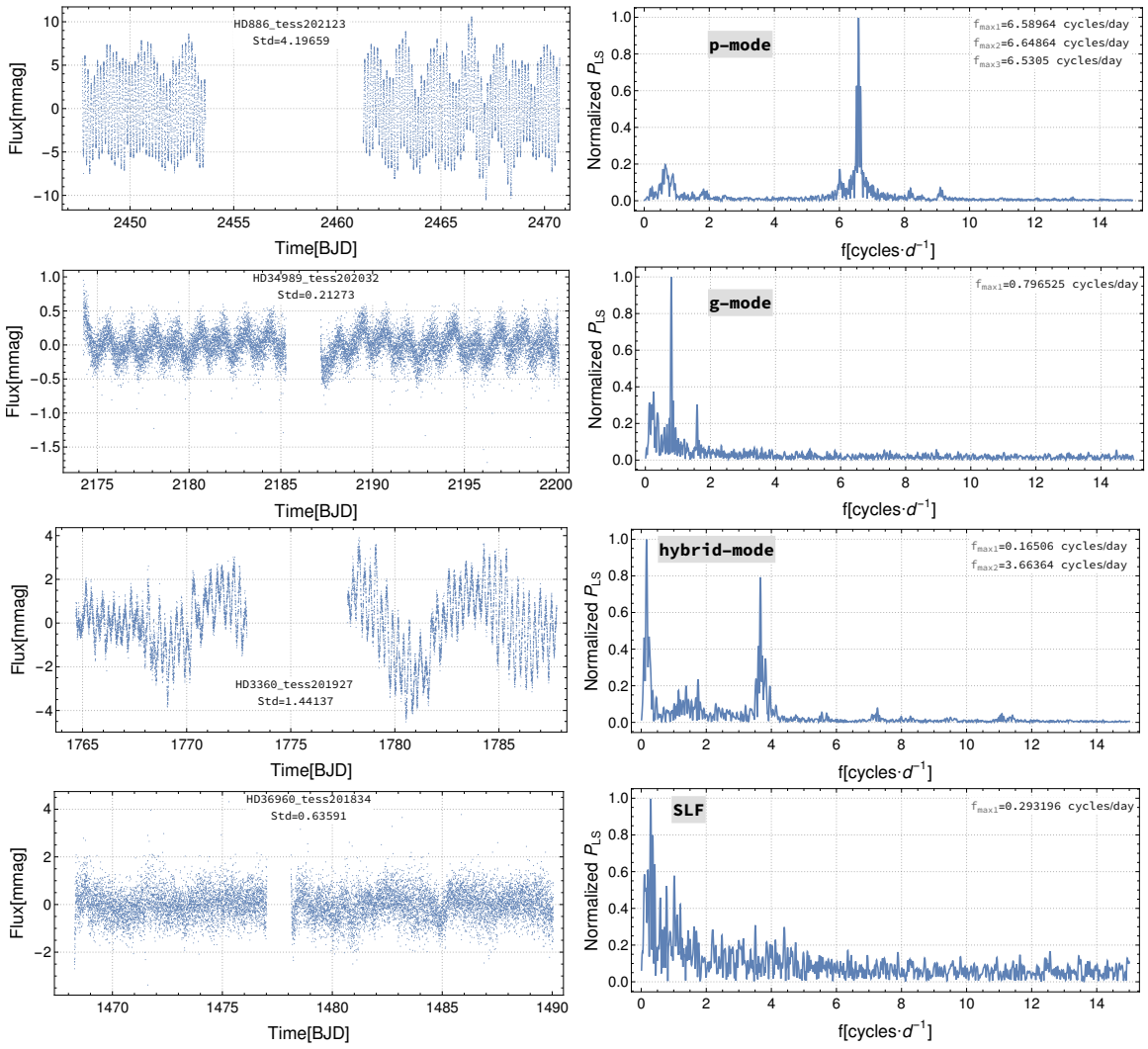

Figure 2.9.: TESS light curves and periodograms for different types of stellar pulsations: p-mod, g-mode, hybrid mode and Stochastic Low Frequency (SLF)

2.5.2. Spectroscopic analysis: binarity

The last technique studied here is an spectroscopic analysis in order to know if the sample stars are part of a binary system and if this could be a cause for them to have a higher nitrogen abundance than expected.

For some of the stars there are more than one spectrum accessible. These spectra are taken in different epochs and shows the brightness of the star at separate times. By plotting all the spectra from a same star together it is likely to observe if it is a binary

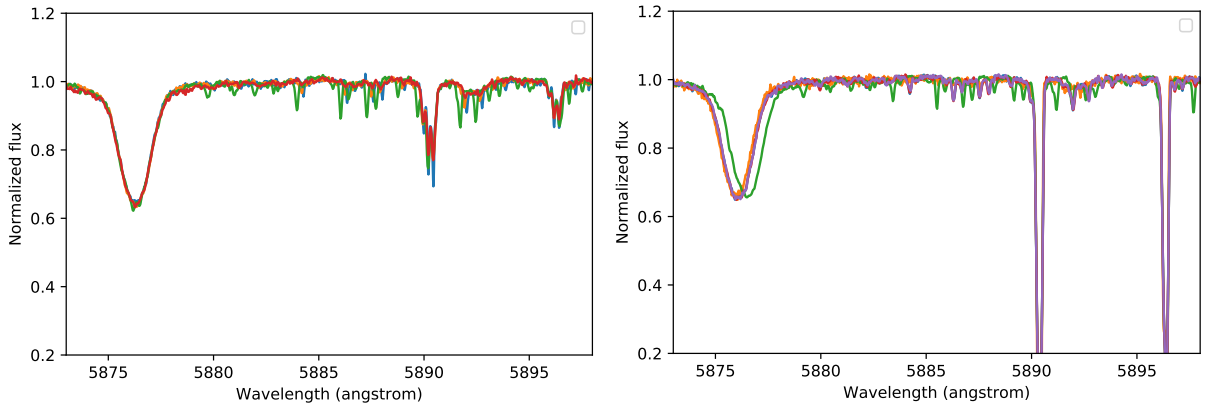

Figure 2.10.: Different epochs spectra for HD37209 (LS) and HD34989 (SB1). The shifting of He I λ5875 Å is probably caused by the binarity of the star.

system or a single star. A total of 46 stars in the sample have 2 or more spectra that allow to do this analysis, but only 17 of them will give a reliable result because only 17 stars have more than 3 spectra. To do so, first all the spectra has to be corrected by heliocentric velocity. By visually inspecting the He I λ5875 Å line profile we can determine if the star is part of a binary system by identifying the existence of any displacement in wavelength of the diagnsotic lines profile. To make sure that the heliocentroc velocity correctoion was correctly performed in all available spectra for a given star we use the He I λ5875 Å interstellar absorption lines. This interstellar lines must always be in the sample position since they do not depend on the star heliocentric velocity. Figure 2.10 shows an example of observed binary system in which the He I λ5875 Å shifting can be clearly seen.

The classification of each star according to this analysis is:

- **SB1**: clear binary system. Some He I λ5875 Å lines appear separated from the others.
- **LS**: likely single. When He I λ5875 Å line is not shifting in wavelenght.
- **LPV**: line-profile variability (Kholtygin et al., 2015). He I λ5875 Å might seem to be moving a bit, but the cause could just be due to pulsations.

3. Results and discussion

3.1. Nitrogen abundances

The conducted analysis explained in 2.4 has led us to the estimation of $T_{\rm eff}$ using three possible ratios of Si lines. With these $T_{\rm eff}$ values and $\log g$ values we have estimated the nitrogen abundances of our stars. As it has been mentioned before, we will consider results obtained with Si II λ6371 Å/Si III λ4552 Å in stars with two or three available ratios. Stars with $T_{\rm eff} \lesssim 25000$ K has been studied using Si II λ6371 Å/Si III λ4552 Å ratio and stars with $T_{\rm eff} \gtrsim 25000$ K have been studied with Si IV λ4116 Å/Si III λ4552 Å ratio. The results obtained for $T_{\rm eff}$, $\log g$, $\xi_{\rm t}$ and log(N/H)+12 are shown in Table 3.1 (complete in Table A.1 in Appendix). Table A.2 in Appendix shows the estimated values for the three different Si ratios.

3.2. Dependence on projected rotational velocity

The first thing done in this work, before even estimating nitrogen abundances, was measuring $v \sin i$ for the star sample as explained in 2.4.1. These results can be plotted together with the log(N/H)+12 results from previous section to see if there is any kind of correlation between both parameters. As we have already explained in the introduction to this work, slow rotating massive stars were not expected to be nitrogen enriched in their surface. In Table A.1 we see that some of the stars have higher nitrogen abundance values than the others. In Fig. 3.1 we investigate whether there exists a correlation between the derived N abundance and the projected rotational velocity of the star (in the so called Hunter plot, Hunter et al., 2008). We have characterized the star sample obtaining the mean and standard deviation of the N abundances for the stars included in 1.7σ($\backsim$33% of the sample) and 2σ($\backsim$78%) of the mean. We have considered as outlayers all stars outside 2σ with high N abundance values ($\backsim$20%), and they have been enumerated to

Table 3.1.: This Table presents a preview of the values estimated by doing a quantitative spectroscopic analysis of the star sample. In the first and second column appears the name and spectral type of the star. In third column we show the effective temperature, $T_{\rm eff}$, with its uncertainty. The surface gravity, $\log g$, is in the fourth column and the uncertainty considered for it is 0.1 dex in all the measures. Microturbulence, $\xi_{\rm t}$, and its corresponding uncertainty is shown in the fifth column. In the sixth column are the nitrogen abundances estimated in this work, with their uncertainties in the seventh column. These N abundance uncertainties includes those originated due to microturbulence, $\xi_{\rm t}$, nitrogen line dispersion, σ and temperature gradient of ΔT=± 500 K. A complete version of this Table is presented in Appendix A.1.

Star Name	**Spec Typ**	**T$_{\rm eff}$ [·10^3 K]**	**log(g) [dex]**	**ξ_t(Micro)**	**log(N/H)+12 [dex]**	**Δlog(N/H) [dex]**		
						ξ	σ	ΔT
HD85953	B2.5III	18.8 ± 0.3	3.6	3.1 ± 2.1	7.70	0.07	0.11	0.12
HD3360	B2IV	20.5 ± 0.3	3.9	4.7 ± 0.8	8.37	0.06	0.07	0.10
HD35039	B2IV	20.0 ± 0.1	3.7	5.3 ± 0.8	7.76	0.03	0.04	0.07
HD42690	B2II	19.0 ± 0.1	3.6	2.4 ± 1.0	7.78	0.03	0.04	0.10
...	...	...	...	...	...	...	...	...

localize them in every plot. In this oulayers we have included star HD205021 as number 10 because it is in the limit of the 2σ region. The percentage of slow rotating stars with high N abundances in this work ($\backsim$20%) is the same as the one obtained by Hunter et al. (2008) for a sample of 135 B-type stars in the Large Magellanic Cloud. Morel et al. (2008) studied a sample of 20 early B-type stars obtaining a mean value of log(N/H)+12=7.67 dex considering not enriched stars. Nieva & Przybilla (2012) did the same for a sample of 29 B-type stars and obtained a mean value of log(N/H)+12=7.79 dex. In our sample, we have a mean of 7.69 dex considering a 1.7 σ and 7.76 dex for 2σ.

If we considered stars with $v \sin i <$ 20 km s^{-1}, only $\backsim$14% of the stars are outlayers with σ>2, so most of these slow rotating stars have low log(N/H)+12 as expected. But if we go to 20-40 km s^{-1} range, almost 30 % of the stars have $\sigma \geq$2, and also considering a mean value of log(N/H)+12=7.76 dex, 56 % of the stars in this range have an abundance higher than 7.86 dex, 0.1 dex more than the mean. The higher the velocity, the higher the

proportion of stars with high nitrogen abundances. If we consider $v \sin i > 40$ km s^{-1} the sample only have 4 stars, not enough to get good statistics, but we see that 25 % of the studied stars are nitrogen enriched. It seems like a greater proportion of enriched stars are expected for high rotational velocities. For slow rotating stars with $v \sin i < 60$ km s^{-1} we expect no N enrichment so studying a larger sample of stars between 20-40 km s^{-1} and specially between 40-60 km s^{-1} will probably reduce the percentage of outlayers.

Also, we cannot forget that some of these stars might be rapid rotators showing a low $v \sin i$ due to the angle i we are seeing them with as explained by Brott et al. (2012) and Aerts et al. (2014).

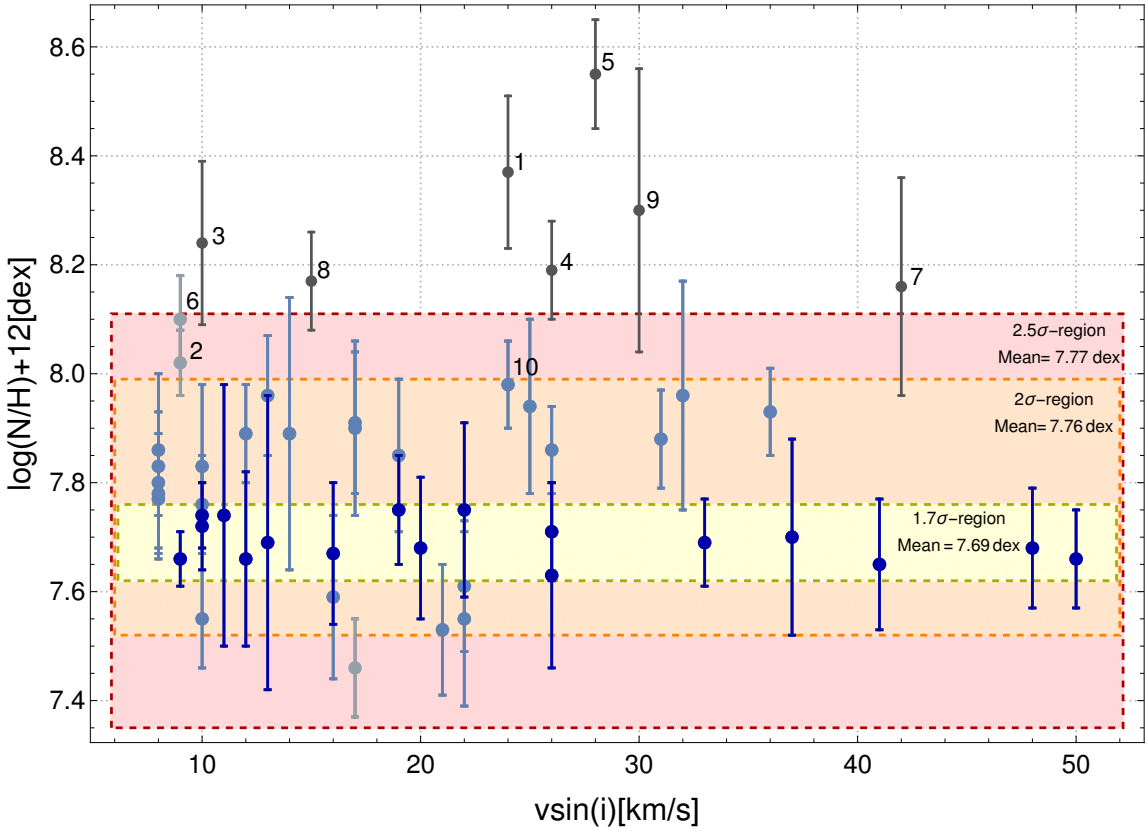

Figure 3.1.: Hunter plot showing the relation between nitrogen abundance and the projected rotational velocity in the considered sample of 51 early-B main sequence stars.

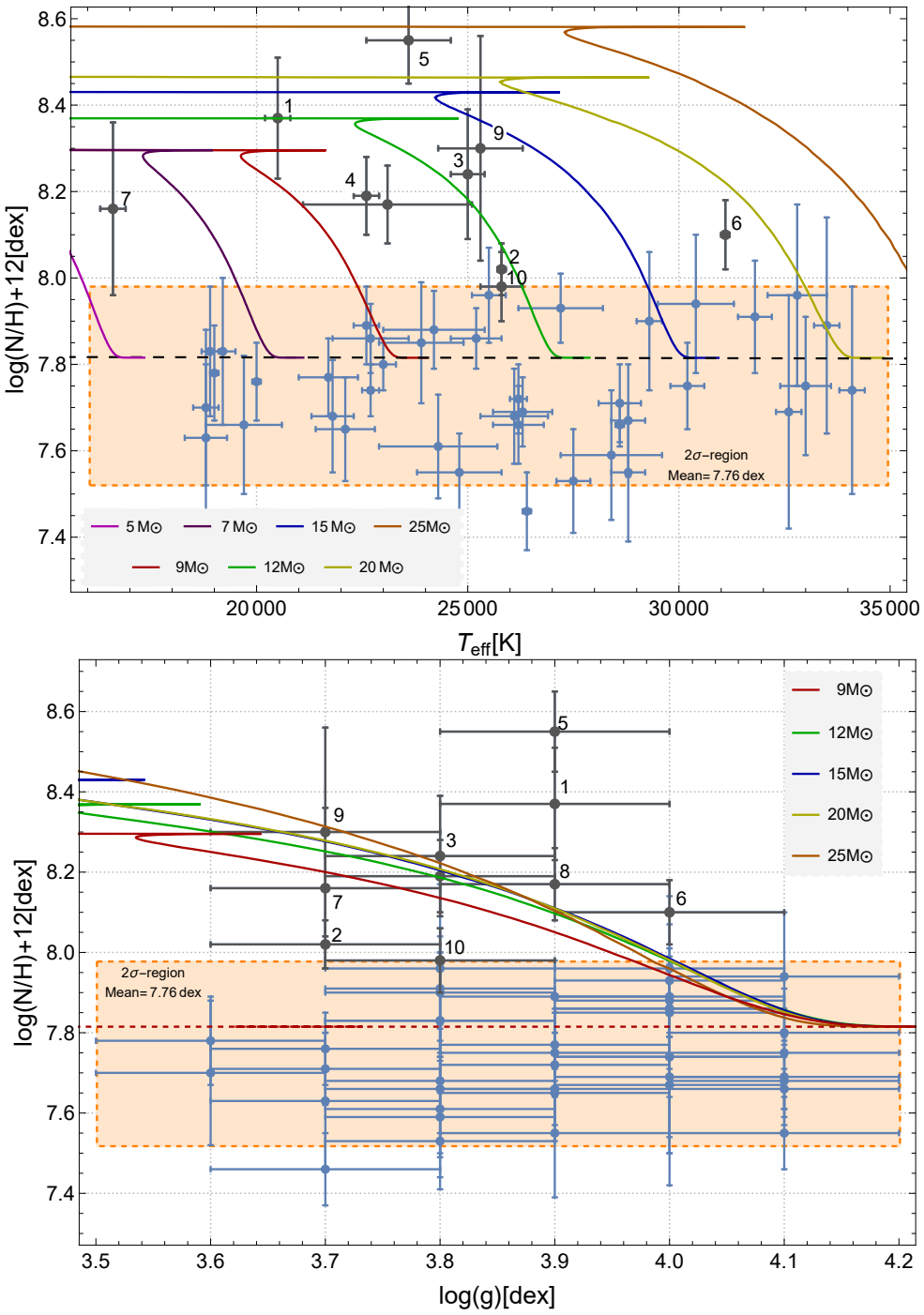

Figure 3.2.: Relation between nitrogen abundance and effective temperature (above) and gravity (below) in the star sample, showing the outlayers in gray. Evolutionary tracks for different masses considering predictions of rotational mixing by Ekström et al. (2012) are shown in different colors. This tracks are made with models with $v \sin i/v_{crit}$=0.4. The evolutionary track for all the masses without considering rotational velocity ($v \sin i/v_{crit}$=0) is shown as a dashed black line with an abundance value of 7.815 dex.

3.3. Dependence on effective temperature and surface gravity

We expect rotational mixing to be more efficient in more massive and more evolved stars. The correlation of N abundances with $T_{\rm eff}$ and $\log g$ will be studied in this Section since $T_{\rm eff}$ is related with the stellar mass and $\log g$ is related with the star evolution. In Fig. 3.2 we show the relation between the nitrogen abundance and the estimated values for $T_{\rm eff}$ and $\log g$. The $T_{\rm eff}$ is directly related with the mass of the star, so studying the relation with the $T_{\rm eff}$ we are studying the relation between nitrogen abundances and the mass of the star. We expected stars with higher $T_{\rm eff}$ (higher masses) to be more enriched, but what we see here is the opposite: the percentage of stars (90%) in the sample with higher values of N is larger for stars with $T_{\rm eff}$ below 25000 K. This happens for all the outlayers except for one (HD149438).

For $\log g$ we expected more enrichment for higher values of the gravity, since this would mean that the most evolved stars have higher N abundance, but we do not see any apparent correlation, The measured $\log g$ values have high uncertainties, so they may differ from the real $\log g$ of the star.

3.4. Variability, oscillations and binarity results

Other mechanisms considered in this study that might be producing nitrogen enrichment in stellar surface of massive slow rotators are the pulsational mixing, the possible binarity in some of them, or their oscillations. How to obtained these parameters was explained in section 2.5, and table 3.2 shows a preview of the results (The complete results are in Table A.3).

Photometric magnitude from TESS light curves has been measured to consider the role of variability in nitrogen enrichment. Also, for the stars in our sample, three different oscillation modes has been observed: the g-mode, the p-mode, and an hybrid-mode whose stars show peaks in both g-mode and p-mode regions. To study the role of these oscillations in the stellar matter mixing we will considered the oscillation frequency of the higher peak measured, those with amplitude equal to 1, since the Lomb-Scargle Periodogram is normalized to the highest peak.

Table 3.2.: This Table presents a preview of the results obtained with the analysis of TESS light curves and periodograms. Second column shows the variability magnitude of the light curve. Frequency values are in the third column, which is divided into three subcolumns: the first one to indicate if the star is SLF (Stochastic Low Frequency), second one to show frequencies of peaks in g-mode, and third one to show frequencies of peaks in p-mode. Some of the stars had more than one light curve available so, in those cases, Table shows all the magnitude and frequency values for each light curve of the star. The fourth column indicates if any contaminant might be affecting the photometric values from TESS. The Fifth column shows the classification of the star according to the binarity. A complete version of this Table is presented in Appendix A.3.

Star Name	$\sigma(T_P)$ [mmag]	Frequency [cycles/day]					Contaminants	Binarity
		SLF	g-mode (f<1)		p-mode (f>1)			
			f [cycles/day]	Amp	f [cycles/day]	Amp		
HD85953	7.80366	NO	0.265543	1	-	-	-	LS(2)
	6.46126	NO	0.263851	1	-	-		
	7.97412	NO	0.2679	1	-	-		
HD3360	1.44137	NO	0.16506	1	3.66364	0.8	NO	LS(2)
HD35039	2.44177	NO	0.357011	1	-	-	-	SBI(12)
			0.26674	0.61				
			0.50962	0.54				
HD42690	2.73695	NO	0.494821	1	-	-	NO	LS(2)
	2.88848	NO	0.535912	1	-	-		
			0.662523	0.87				
			0.346069	0.6				
...	...	...	...	...	...	...	...	...

Table A.3 also shows the classification of each star according to their binarity as described in section 2.5.2. We have considered if there are contaminants nearby the star that could be altering the photometric observations made by TESS or the spectra used in this work since this could also affect our results. This has been done using the Washington Double Star Catalog from VizieR.

For some of the star it was not possible to study the oscillations since these were not accessible in MAST. Even though there were TESS data for all the stars, some of them have not been extracted from the Full Frame Image (FFI) yet, and their light curves are

not available. This study would greatly benefits from the increase of available data and new observations from TESS.

3.5. Dependence on the pulsational properties

With the values in table A.3 we can study the role that pulsatonal mixing plays in the nitrogen enrichment. Figure 3.4 shows log(N/H)+12 as a function of the frequency of oscillation and as a function of the amplitude of photometric variability measured for the TESS light curves. In the two plots we have marked with different symbols/colors those stars in which the dominant frequency is located in the p- or g-mode domain (or whether it is an hybrid pulsator).

When comparing oscillation frequencies and nitrogen abundances we do not see any correlation. It can be seen that 40% of the outlayers have p-mode oscillations. These p-mode outlayers also have high amplitudes over 6 mmag. In case of g-mode oscillations just a 20% of the outlayers present this pulsations, and their amplitudes are lower than 4 mmag. There is also a 20% of outlayers that with Stochastic Low Frequency (SLF) and whose magnitudes are really small (lower than 1.5 mmag). There is one star (10% of the outlayers) that presents and hybrid mode and a low variability amplitud. Considering the whole sample, there is no difference in frequency for SLF, g-mode and hybrid mode oscillations.

As it was already commented in the introduction, g-mode pulsations (or hybrid mode with main peak in the g-mode region) might be transferring core material to the outer layers making the surface to have more nitrogen than it should have, while p-mode pulsations should not be playing an important role since they would only mix matter between internal layers, but not from core to the surface. What we observe in our star sample is that almost half of the enriched stars have p-mode oscillations, while only the 20 % of them has g-mode oscillations, contrary to what we expected at first. Also, all p-mode stars has a log(N/H)+12 higher than the mean except for one. This might imply that p-mode oscillations are playing a role in nitrogen enrichment in the stellar surface, but this would not be the only mechanism involved.

The study of the amplitude of variability barely shows a correlation. We observe that some of the g-mode stars have high magnitudes compare to the rest of g-mode stars. For SLF, the amplitudes are also very low. The variability magnitude for stars with p-

mode oscillations are always higher than 4 mmag. We expect more N abundance for high magnitude, which can be observed in outlayers with p-mode oscillations, and also in one of the stars with a g-mode oscillation.

Figure 3.3 shows the Kiel diagram of the studied stars considering the different kind of oscillations explained before.

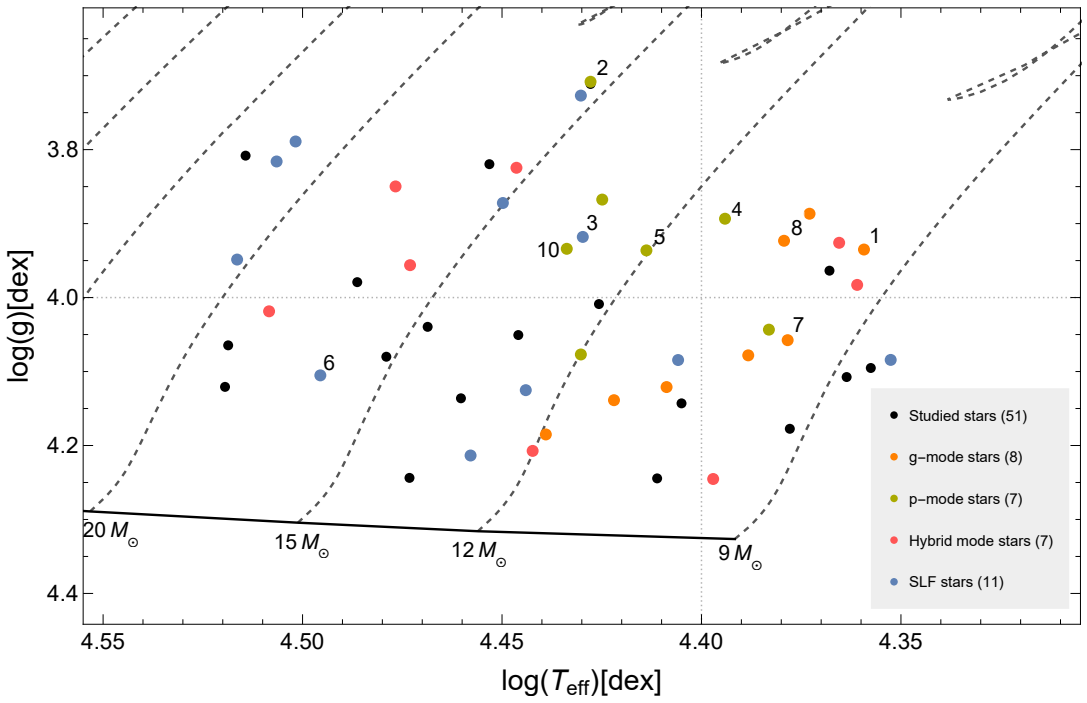

Figure 3.3.: Kiel Diagram for the whole sample of stars considered in this study showing the different type of pulsation for each star.

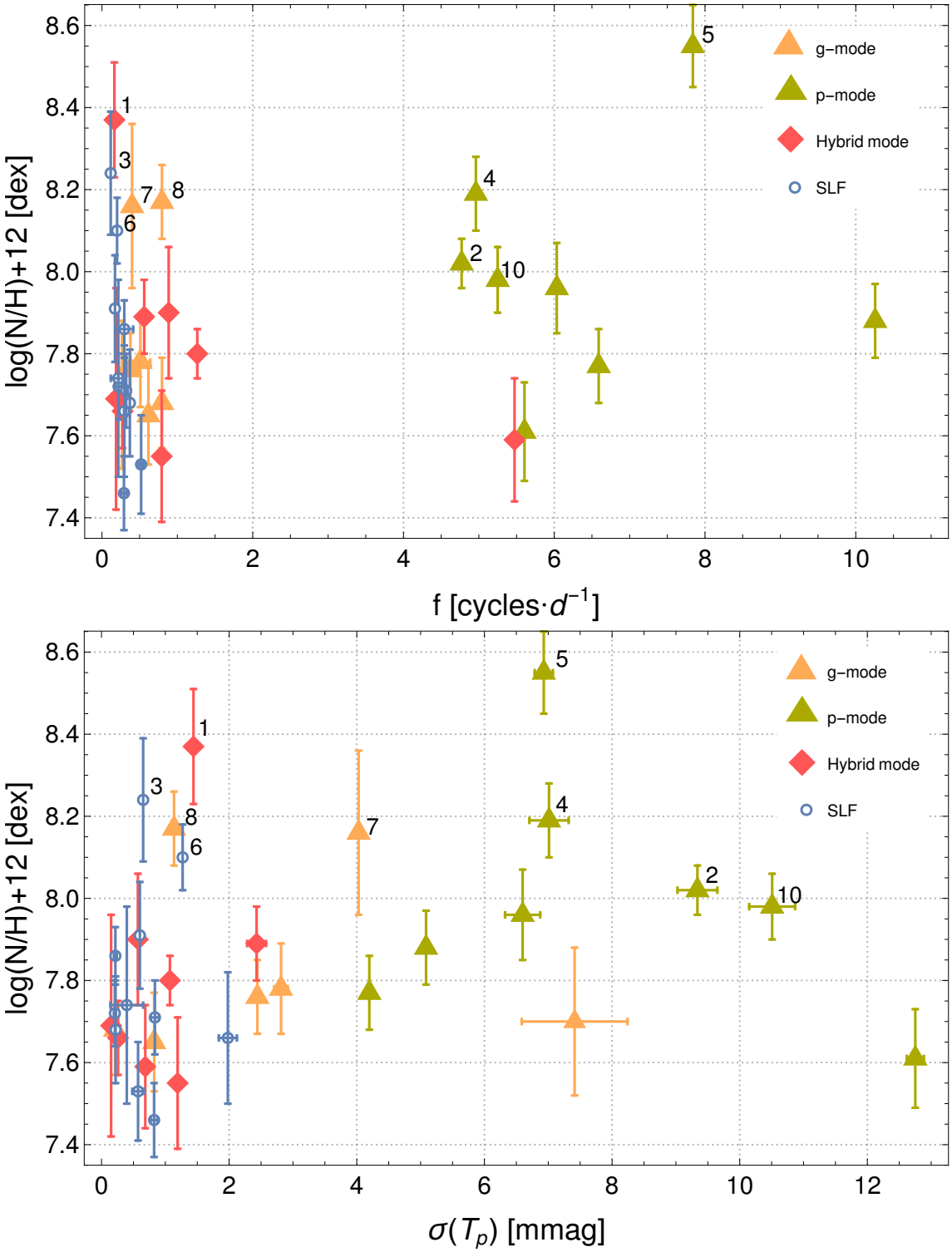

Figure 3.4.: Periodogram frequencies and Standard deviation in comparison with nitrogen abundances.

3.6. Dependence on magnetic fields

Magnetic field effect is another mechanism already studied by Morel et al. (2008) and Przybilla & Nieva (2011) that could be a cause for nitrogen enrichment. Some stars in the studied sample have magnetic fields that have been detected and interpreted. For the rest of the stars their magnetic field has not been detected yet or else they do not have one. We have collect magnetic field information from two surveys: FORS1 observations (Bagnulo et al., 2015) and MiMeS (Wade et al., 2016). This two surveys has measured the magnetic field in three directions: B_x, B_y and B_z, being the last of them the magnetic field measured in the direction of the line of sight. Figure 3.5 shows log(N/H)+12 as a function of B_z for the two set of measures.

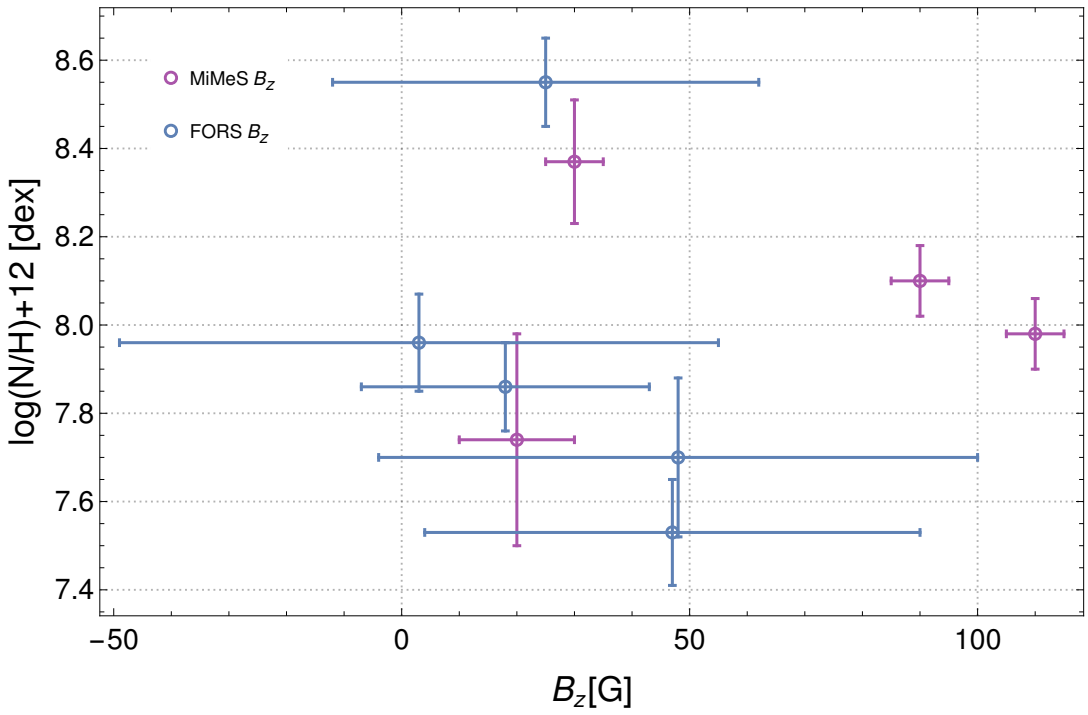

Figure 3.5.: Literature magnetic fields in comparison with nitrogen abundances.

Half of the stars with log(N/H)+12>7.96 have a magnetic field, and all the stars that appears to be magnetic have a log(N/H)+12 higher than the mean, except for one single star (HD36960). The rest of the star with low abundances have no magnetic field or has not been yet measured. This means that magnetic stars have some chemical peculiarities

as Morel et al. (2008) already observed. It is not possible to get a correlation, only than magnetic field is appearing in nitrogen enriched stars, while it has not been measured in not-enriched stars (except for HD36960). These magnetic fields in star could be slowing down the star, making fast rotators become into slow rotators.

3.7. Comments on individual outlayer objects

1. ***HD3360*** has a log(N/H)+12=8.37 dex. Calculations of $T_{\rm eff}$ and $\log g$ agree with those of Nieva & Przybilla (2012) that also studied this star, but the N abundance obtained here is a bit higher. This star has a $v \sin i$ of 25 km s^{-1} and is one of the stars in 20-40 km s^{-1} range commented before, that appears to have a greater proportion of enriched stars. HD3360 also has hybrid-mode oscillations, with the main peak at a frequency of 0.17 cycles/d and a p-mode peak of 80 % of amplitude at a frequency of 3.7 cycles/d. As mention before, this p-mode oscillations might be playing a role in the enrichment of this star. No binary system or contamination were observed for this star, but the magnetic field was measured by MiMeS Survey.

The nitrogen enrichment might be produced by a combination of g-mode and p-mode oscillations and the presence of magnetic field.

2. ***HD46328*** has a log(N/H)+12=8.02 dex. This star is a slow rotator with $v \sin i$=8 km s^{-1} and have p-mode oscillations at frequency of 4.7 cycles/d. The $\sigma(T_P)$ is higher than 9 mmag. This star has been classify as a SB1, so it is a binary star. The only observed mechanism that could be producing the matter mixing in the star are the p-mode oscillations but the binarity of the star has to be considered too.

3. ***HD59882*** has a log(N/H)+12=8.24 dex and rotates with $v \sin i$=10 km s^{-1}. This star is SLF (Stochastic low frequency), with his higher peak at frequency 0.12 cycles/d. It was not possible to check if it is part of a binary system and no magnetic field has been measured. Nothing seems to explain the nitrogen enrichment in this star, so two possibilities might be considered: the nitrogen estimation was done wrongly (unprobably) or we are observing this star with an small i angle.

4. ***HD64365*** has a log(N/H)+12=8.19 dex and $v \sin i$=26 km s^{-1}. This star has p-mode oscillations at frequency 4.96 cycles/d and no study of the binarity could be done. The standard deviation in the light curve is around 7 mmag. No magnetic field has been detected. The only mechanism studied that could be playing a role in this star are the

p-mode oscillations.

5. *HD129557* has a log(N/H)+12=8.55 dex, the highest one measured, and $v \sin i$=28 km s^{-1}. This star also has an standard deviation of around 7 mmag in its light curves, and presents p-mode oscillations at a frequency of 7.8 cycles/d. No binarity studies could be made, but FORS1 could measure its magnetic field. As other stars, the mechanism that could be producing the nitrogen enrichment are p-modes oscillations and/or magnetic field effects.

6. *HD149438(τ Sco)* has a log(N/H)+12=8.10 dex and a $v \sin i$=9km s^{-1}. Its nitrogen abundance was also estimated by both Morel et al. (2008) and Nieva & Przybilla (2012), and a similir but slighly smaller result was obtained in this work. This star is a SLF and it the study of its multiepoch spectra show that it is likely single star. The MiMeS Survey provided a value for its magnetic field, being this the only possible mechanism producing the nitrogen enrichment.

7. *HD162374* has a log(N/H)+12=8.16 dex and a $v \sin i$=42km s^{-1}. The uncertainties introduced by temperature (Δlog (N/H)$_{\Delta T}$=0.17 dex) are really high in this case. A wrong estimation of $T_{\rm eff}$ might have affected this result. This star has a standard deviation of 4 mmag and g-mode oscillations at frequency 0.4 cycles/d. No binarity conclusions could be made here, and no magnetic field has been detected. The only possible mechanism here are the g-mode oscillations, but this star being an enriched star might be just an estimation error.

8. *HD197512* has a log(N/H)+12=8.17 dex and a $v \sin i$=15km s^{-1}. This star has g-mode oscillations at frequency 0.8 cycles/d and is likely single. No magnetic field has been found. The only possible explanation for the enrichment are g-mode oscillations.

9. *HD201638* has a log(N/H)+12=8.30 dex and a $v \sin i$=30km s^{-1}. No photometric data or magnetic field were available for this star. Spectra show it to be likely single. No explanation are found for this star enrichment.

10. *HD205021* has a log(N/H)+12=7.98 dex and a $v \sin i$=30km s^{-1}. Measures made by Nieva & Przybilla (2012) and Morel et al. (2008) are a bit higher than in this work. It has a high standard deviation of 10 mmag and p-modes oscillations at 5.2 cycled/d. This star also appears to be a binary system, altough some contaminants were found that could be affecting the spectra. Also, MiMeS found a strong magnetic field over 100 G in this star. All possibles mechanism studied hear appear in this star.

4. Conclusions

Different mechanism have been studied throughout this work to explain the reason for some massive star to have high nitrogen abundances in their surface. It was already seen that velocity does not play a role in here, since slow rotating massive stars also have high nitrogen abundances in some case, even if their projected rotational velocity is too low. This has been observed also here in this work, there is no apparent correlation between velocity and the nitrogen estimated, at least in the sample of stars studied here. Also, gravity does not seem to be a mechanism that could be affect this situation, but if we consider the effective temperature, $T_{\rm eff}$, we have seen that nitrogen enriched stars are part of the cold stars ($T_{\rm eff} \leq 25000$ K), while only one hot star ($T_{\rm eff} > 30000$ K) is enriched in its surface. This means that stars with lower masses are more enriched than the more massive stars.

Other mechanism studied in this work is the pulsational mixing in the stars. Considering the oscillations of the stellar interior, more than half of the enriched stars whose oscillations could be measured have shown p-modes oscillations. This is unexpected, since g-modes oscillations are believed to be the one that transfer matter from core to the surface, while p-modes oscillations take place in the convective zone mixing the matter in the boundaries between stellar layers. There are two stars with high nitrogen abundances whose only explanation for it are the g-modes oscillations taking place in their interior, while enriched stars with p-modes oscillations also has another studied mechanism occurring in the star. Gravity-modes oscillations could be producing the matter transfer to the surface by themselves, while p-mode oscillations play a role in this but with help of another process. There is neither a correlation seen when considering the amplitudes of the light curves. Nitrogen enriched stars has amplitudes of photometric variability with values going from 0.2 mmag to 10 mmag, while non-enriched stars also appear in the whole range of values.

A spectroscopic study has been done too to check if any of our stars might be part of

a binary system. Only two of the ten enriched stars could be a binary system so binarity does not play an important role here neither.

The last mechanism studied in this work is the magnetic field. There was not enough data to have a good statistic, but even though we have seen that stars whose magnetic field has been detected also has a nitrogen abundance in their surface higher than the mean value and this magnetic field could explain the enrichment in at least four stars, but it is not so clear.

Better results could be obtained with a more detailed study following the previous work done here and with more access to new data. The initial star sample had to be reduced due to the lack of observation for some of the stars, and the following sample also was reduced due to the difficulties to measure their nitrogen abundance because of their lack of nitrogen spectral lines. The study of some processes was possible thanks to the available TESS observations, but this observational data was not reduced yet by TESS pipeline for some of our stars. New tools are being developed to solve this and work with all the data from TESS, which in the future will be very beneficial to continue this work and to gain more information about variability and oscillations in the stars.

Bibliography

Aerts, C., Christensen-Dalsgaard, J. & Kurtz, D. W. Asteroseismology, (Springer-Verlag, ed 1, 2010)

Aerts, C., Molenberghs, G., Kenward, M. & Neiner, C. The Surface Nitrogen Abundance of a Massive Star in Relation to its Oscillations, Rotation, and Magnetic Field. *ApJ.* **781**, e88 (2014,2)

Aerts, C. & Rogers, T. Observational Signatures of Convectively Driven Waves in Massive Stars. *ApJ.* **806**, eL33 (2015,6)

Bagnulo, S., Fossati, L., Landstreet, J. & Izzo, C. The FORS1 catalogue of stellar magnetic field measurements. *A&A.* **583** pp. eA115 (2015,11)

Beck, P., Montalban, J., Kallinger, T. et al. Fast core rotation in red-giant stars as revealed by gravity-dominated mixed modes. . **481**, 55-57 (2012,1)

Bedding, T., Mosser, B., Huber, D. et al. Gravity modes as a way to distinguish between hydrogen- and helium-burning red giant stars. . **471**, 608-611 (2011,3)

Brott, I., Evans, C., Hunter, I., et al. Rotating massive main-sequence stars. II. Simulating a population of LMC early B-type stars as a test of rotational mixing. *A&A.* **530** pp. eA116 (2011,6)

Burssens, S., Simón-Díaz, S., Bowman, D., et al. Variability of OB stars from TESS southern Sectors 1-13 and high-resolution IACOB and OWN spectroscopy. *A&A.* **639** pp. eA81 (2020,7)

Dufton, P., Thompson, A., Crowther, P., Evans, C., et al. The VLT-FLAMES Tarantula Survey. XXVIII. Nitrogen abundances for apparently single dwarf and giant B-type stars with small projected rotational velocities. *A&A.* **615** pp. eA101 (2018,7)

Dufton, P., Evans, C., Lennon, D. & Hunter, I. The NGC 346 massive star census. Nitrogen abundances for apparently single, narrow lined, hydrogen core burning B-type stars. *A&A*. **634** pp. eA6 (2020,2)

Ekström, S., Georgy, C., Eggenberger, P. et al. Grids of stellar models with rotation. I. Models from 0.8 to 120 M_⊙ at solar metallicity (Z = 0.014). *A&A*. **537** pp. eA146 (2012,1)

Evans, C., Smartt, S., Lennon, D. et al. The VLT-FLAMES Survey of Massive Stars. *The Messenger*. **122** pp. 36-38 (2005,12)

Heger, A. & Langer, N. Presupernova Evolution of Rotating Massive Stars. II. Evolution of the Surface Properties. *ApJ*. **544**, 1016-1035 (2000,12)

Herrero, A., Kudritzki, R., Vilchez, J. et al. Intrinsic parameters of galactic luminous OB stars.. *A&A*. **261** pp. 209-234 (1992,7)

Holgado, G., Simón-Díaz, S., Barbá, R., et al. The IACOB project. V. Spectroscopic parameters of the O-type stars in the modern grid of standards for spectral classification. *A&A*. **613** pp. eA65 (2018,6)

Hunter, I., Brott, I., Lennon, D., et al. The VLT FLAMES Survey of Massive Stars: Rotation and Nitrogen Enrichment as the Key to Understanding Massive Star Evolution. *ApJ*. **676**, L29 (2008,3)

Kholtygin, A., Sudnik, N. & Dushin, V. Line profile variability in spectra of hot massive stars. *New Windows On Massive Stars*. **307** pp. 113-114 (2015,1)

Langer, N. Helium enrichment in massive early type stars. *A&A*. **265** pp. L17-L20 (1992,11)

Lichtblau, D. "Estimating Variable Star Periods from Unevenly Sampled Light Curve Data" from the Notebook Archive (2006), https://notebookarchive.org/2018-07-6z257h4

Lomb, N. Least-squares frequency analysis of unequally spaced data. *Astrophysics And Space Science*. **39**, 447-462 (1976,2,1), https://doi.org/10.1007/BF00648343

Meynet, G. & Maeder, A. Stellar evolution with rotation. V. Changes in all the outputs of massive star models. *A&A*. **361** pp. 101-120 (2000,9)

Morel, T., Hubrig, S. & Briquet, M. Nitrogen enrichment, boron depletion and magnetic fields in slowly-rotating B-type dwarfs. *A&A*. **481**, 453-463 (2008,4)

Nieva, M. & Przybilla, N. Present-day cosmic abundances. A comprehensive study of nearby early B-type stars and implications for stellar and Galactic evolution and interstellar dust models. *A&A*. **539** pp. eA143 (2012,3)

Przybilla, N. & Nieva, M. Mixing of CNO-cycled matter in pulsationally and magnetically active massive stars. *Active OB Stars: Structure, Evolution, Mass Loss, And Critical Limits*. **272** pp. 26-31 (2011,7)

Puls, J., Urbaneja, M., Venero, R., et al. Atmospheric NLTE-models for the spectroscopic analysis of blue stars with winds. II. Line-blanketed models. *A&A*. **435**, 669-698 (2005,5)

Ricker, G., Winn, J., Vanderspek, R. et al. Transiting Exoplanet Survey Satellite (TESS). *Space Telescopes And Instrumentation 2014: Optical, Infrared, And Millimeter Wave*. **9143** pp. e914320 (2014,8)

Rivero González, J., Puls, J., Najarro, F. & Brott, I. Nitrogen line spectroscopy of O-stars. II. Surface nitrogen abundances for O-stars in the Large Magellanic Cloud. *A&A*. **537** pp. eA79 (2012,1)

Sana, H., De Mink, S., De Koter, A. et al. Binary Interaction Dominates the Evolution of Massive Stars. *Science*. **337**, 444 (2012,7)

Scargle, J. Studies in astronomical time series analysis. II. Statistical aspects of spectral analysis of unevenly spaced data.. *ApJ*. **263** pp. 835-853 (1982,12)

Simón-Díaz, S. & Herrero, A. Fourier method of determining the rotational velocities in OB stars. *A&A*. **468**, 1063-1073 (2007,6)

Simón-Díaz, S. The chemical composition of the Orion star forming region. I. Homogeneity of O and Si abundances in B-type stars. *A&A*. **510** pp. eA22 (2010,2)

Simón-Díaz, S., Castro, N., Herrero, A. et al. The IACOB project: A grid-based automatic tool for the quantitative spectroscopic analysis of O-stars. *Journal Of Physics Conference Series*. **328** pp. e012021 (2011,12)

Simón-Díaz, S. & Herrero, A. The IACOB project. I. Rotational velocities in northern Galactic O- and early B-type stars revisited. The impact of other sources of line-broadening. *A&A*. **562** pp. eA135 (2014,2)

Simón-Díaz, S., Pérez Prieto, J., Holgado, G., et al. The IACOB spectroscopic database. New interface and second data release. *XIV.0 Scientific Meeting (virtual) Of The Spanish Astronomical Society*. pp. e187 (2020,7)

Telting, J., Schrijvers, C., Ilyin, I., et al. A high-resolution spectroscopy survey of β Cephei pulsations in bright stars. *A&A*. **452**, 945-953 (2006,6)

VanderPlas, J. Understanding the Lomb–Scargle Periodogram. *The Astrophysical Journal Supplement Series*. **236**, 16 (2018,5,11), http://dx.doi.org/10.3847/1538-4365/aab766

Wade, G., NeinerC., Alecian, E. et al. The MiMeS survey of magnetism in massive stars: introduction and overview. *MNRAS*. **456**, 2-22 (2016,2)

Walborn, N. The OBN and OBC stars.. *ApJ*. **205** pp. 419-425 (1976,4)

Walborn, N. Evolutionary Helium and CNO Anomalies in the Atmospheres and Winds of Massive Hot Stars. *IAU Colloq. 108: Atmospheric Diagnostics Of Stellar Evolution*. **305** pp. 70 (1988)

This research has made use of the VizieR catalogue access tool, CDS, Strasbourg, France (DOI : 10.26093/cds/vizier). The original description of the VizieR service was published in 2000, A&AS 143, 23

A. Appendix I: Tables

A.1. Nitrogen abundances

Table A.1.: This Table presents all the values estimated by doing a quantitative spectroscopic analysis of the star sample. In the first and second column appears the name and spectral type of the star. In third column we show the effective temperature, $T_{\rm eff}$, with it uncertainty. The surface gravity, $\log g$, is in the fourth column and the uncertainty considered for it is 0.1 dex in all the measures. Microturbulence, $\xi_{\rm t}$, and its corresponding uncertainty is shown in the fifth column. In sixth column are the nitrogen abundances estimated in this work, with their uncertainties in the seventh column. These N abundance uncertainties includes those originated due to microturbulence, $\xi_{\rm t}$, nitrogen line dispersion, σ and temperature gradient of ΔT=$\pm$ 500 K.

Star Name	**Spec Typ**	**T$_{\rm eff}$ [$\cdot 10^3$ K]**	**log(g) [dex]**	**ξ(Micro)**	**log(N/H)+12 [dex]**	**Δlog(N/H) [dex]**		
						ξ	σ	ΔT
HD85953	B2.5III	18.8 $\pm$ 0.3	3.6	3.1 $\pm$ 2.1	7.70	0.07	0.11	0.12
HD3360	B2IV	20.5 $\pm$ 0.3	3.9	4.7 $\pm$ 0.8	8.37	0.06	0.07	0.10
HD35039	B2IV	20.0 $\pm$ 0.1	3.7	5.3 $\pm$ 0.8	7.76	0.03	0.04	0.07
HD42690	B2II	19.0 $\pm$ 0.1	3.6	2.4 $\pm$ 1.0	7.78	0.03	0.04	0.10
HD157056	B2IV	22.7 $\pm$ 0.9	4.0	1.9 $\pm$ 0.8	7.86	0.03	0.05	0.05
HD886	B2IV	21.7 $\pm$ 0.1	3.9	1.6 $\pm$ 0.5	7.77	0.01	0.05	0.07
HD253049	B2IV	19.7 $\pm$ 0.9	3.8	4.1 $\pm$ 3.2	7.66	0.09	0.08	0.10
HD60553	B2II	23.9 $\pm$ 1.0	4.0	3.7 $\pm$ 2.8	7.85	0.11	0.09	0.02
HD223128	B2IV	22.6 $\pm$ 0.3	3.9	2.4 $\pm$ 1.4	7.89	0.06	0.03	0.06
HD829	B3III	18.9 $\pm$ 0.2	3.8	2.9 $\pm$ 2.0	7.83	0.05	0.07	0.12
HD77770	B2IV	18.8 $\pm$ 0.5	3.7	3.8 $\pm$ 3.0	7.63	0.10	0.04	0.13
HD162374	B6Ib	16.6 $\pm$ 0.3	3.7	4.2 $\pm$ 3.5	8.16	0.11	0.03	0.17
HD174298	B1.5V	24.2 $\pm$ 1.2	4.0	2.1 $\pm$ 1.0	7.88	0.06	0.06	0.02
HD64365	B2III	22.6 $\pm$ 0.3	3.8	2.5 $\pm$ 0.9	8.19	0.05	0.06	0.05
HD158304	B3III	19.2 $\pm$ 0.3	3.8	5.3 $\pm$ 4.1	7.83	0.11	0.06	0.11
HD37356	B3V	21.8 $\pm$ 0.5	3.8	5.8 $\pm$ 4.5	7.68	0.08	0.03	0.10
HD220172	B3II	22.1 $\pm$ 0.7	3.9	3.3 $\pm$ 2.5	7.65	0.08	0.06	0.06

Star Name	Spec Typ	T_{eff} [$\cdot 10^3$ K]	log(g) [dex]	ξ(Micro)	log(N/H)+12 [dex]	Δlog(N/H) [dex]		
						ξ	σ	ΔT
HD35299	B2III	23.0 ± 0.3	4.1	3.0 ± 0.6	7.80	0.02	0.05	0.03
HD197512	B2III	23.1 ± 2.0	3.9	3.4 ± 1.0	8.17	0.06	0.05	0.04
HD35337	B2III	22.7 ± 0.2	4.0	1.5 ± 0.5	7.74	0.03	0.03	0.04
HD43112	B2III	25.2 ± 0.6	4.0	2.6 ± 0.8	7.86	0.03	0.05	0.04
CPD573524B	B1V	24.3 ± 1.4	3.8	6.4 ± 2.3	7.61	0.08	0.09	0.01
HD205021	B0.5IIIs	25.8 ± 0.5	3.8	1.9 ± 0.5	7.98	0.02	0.07	0.04
HD36591	B2II/III	26.2 ± 0.2	3.9	1.5 ± 0.5	7.72	0.01	0.07	0.04
HD36960	B1/2Ib/II	27.5 ± 0.4	3.8	5.5 ± 4.0	7.53	0.06	0.08	0.06
HD201795	B1V	28.6 ± 0.1	4.1	2.1 ± 0.6	7.66	0.01	0.04	0.03
HD34816	B0.5V	28.8 ± 0.4	3.9	6.1 ± 3.4	7.55	0.09	0.12	0.06
HD36822	B0III	29.3 ± 0.3	3.8	4.6 ± 2.5	7.90	0.07	0.12	0.07
HD119069	B3II	28.8 ± 0.4	4.0	5.8 ± 3.2	7.67	0.06	0.10	0.05
HD149438	B0.2V	31.1 ± 0.1	4.0	3.2 ± 0.5	8.10	0.01	0.05	0.06
HD202214	O9.5IV	28.6 ± 0.5	3.7	2.3 ± 1.3	7.71	0.02	0.08	0.04
HD46328	B0.7IV	25.8 ± 0.1	3.7	2.9 ± 0.5	8.02	0.02	0.07	0.05
HD61068	B2II	25.5 ± 0.4	4.0	2.0 ± 0.8	7.96	0.04	0.10	0.03
HD36512	O9.7V	32.6 ± 0.3	4.0	5.3 ± 2.8	7.69	0.03	0.22	0.16
HD166523	B3II	27.2 ± 1.0	4.0	2.2 ± 1.1	7.93	0.04	0.05	0.04
HD59882	B2Ib/II	25.0 ± 0.4	3.8	2.9 ± 0.8	8.24	0.05	0.14	0.02
HD255134	B1IVp	26.4 ± 0.1	3.7	4.6 ± 5.0	7.46	0.07	0.03	0.04
HD34989	B1V	26.1 ± 0.8	4.1	2.1 ± 1.0	7.68	0.03	0.10	0.03
HD37209	B3IV	26.2 ± 0.6	3.9	6.5 ± 2.3	7.66	0.03	0.09	0.01
HD54025	B2II	24.8 ± 1.0	4.1	2.5 ± 1.8	7.55	0.04	0.07	0.04
HD129557	B2III	23.6 ± 1.0	3.9	2.0 ± 0.8	8.55	0.05	0.08	0.03
HD251847	B1IV	28.4 ± 1.2	3.8	12.1 ± 2.3	7.59	0.03	0.15	0.01
HD201638	B0.5Ib	25.3 ± 1.0	3.7	6.3 ± 4.3	8.3	0.24	0.11	0.03
HD211880	B0.5V	30.4 ± 0.9	4.1	4.4 ± 3.5	7.94	0.08	0.13	0.05
HD164704	B2II	26.3 ± 0.7	4.1	2.9 ± 1.9	7.69	0.06	0.05	0.03
HD165016	B2Ib	30.2 ± 0.4	3.9	2.1 ± 1.0	7.75	0.01	0.07	0.07
HD192039	B0IV	31.8 ± 0.4	3.8	5.4 ± 4.1	7.91	0.05	0.07	0.10
HD166539	B1/2Ib	32.8 ± 0.7	3.8	2.2 ± 0.7	7.96	0.01	0.10	0.19
HD34078	O9.5V	34.1 ± 0.3	4.0	4.5 ± 2.7	7.74	0.02	0.20	0.13
HD206183	O9.5IV-V	33.5 ± 0.3	4.0	4.2 ± 2.7	7.89	0.03	0.21	0.13
HD161789	B2/3II	33.0 ± 0.6	4.1	1.7 ± 0.6	7.75	0.01	0.15	0.05

A.2. Previous nitrogen abundance estimation

Table A.2.: This Table presents the values estimated by doing a quantitative spectroscopic analysis of the star sample considering all the possible Si ratios. In the first and second column appears the name and spectral type of the star. In third column we show the effective temperature, $T_{\rm eff}$, with its uncertainty. The surface gravity, $\log g$, is in the fourth column and the uncertainty considered for it is 0.1 dex in all the measures. Microturbulence, $\xi_{\rm t}$, and its corresponding uncertainty is shown in the fifth column. In sixth column are the nitrogen abundances estimated in this work, with their uncertainties in the seventh, eight and nineth column. These N abundance uncertainties includes those originated due to microturbulence, $\xi_{\rm t}$, nitrogen line dispersion, σ and temperature gradient of ΔT=$\pm$ 500 K. The different ratios are shown in the Table as: Si IV λ4116 Å/Si III λ4552 Å (A), Si II λ4128 Å/Si III λ4552 Å (B), Si II λ6371 Å/Si III λ4552 Å (C).

Star Name	Spec Typ	$T_{\rm eff}$[$\cdot 10^3$ K]			Logg			ξ(Microturbulence)			Log(N/H)+12 [dex]			ΔLog(N/H)$_{\xi}$ [dex]			ΔLog(N/H)$_{\rm dis}$ [dex]			ΔLog(N/H)$_{\rm T}$ [dex]		
		A	B	C	A	B	C	A	B	C	A	B	C	A	B	C	A	B	C	A	B	C
HD85953	B2.5III	-	19.2 (0.3)	18.8 (0.3)	-	3.7	3.6	-	3.2 (2.1)	3.1 (2.1)	-	7.67	7.70	-	0.07	0.07	-	0.11	0.11	-	0.12	0.12
HD3360	B2IV	-	22.8 (0.3)	20.5 (0.3)	-	3.9	3.9	-	1.8 (0.6)	4.7 (0.8)	-	8.14	8.37	-	0.03	0.06	-	0.02	0.07	-	0.05	0.10
HD35039	B2IV	-	22.0 (0.2)	20.0 (0.1)	-	3.8	3.7	-	1.3 (0.2)	5.3 (0.8)	-	7.62	7.76	-	0.01	0.03	-	0.04	0.04	-	0.14	0.07
HD42690	B2II	-	21.6 (0.1)	19.0 (0.1)	-	3.9	3.6	-	2.0 (0.9)	2.4 (1.0)	-	7.52	7.78	-	0.02	0.03	-	0.02	0.04	-	0.08	0.10
HD157056	B2IV	-	24.7 (0.6)	22.7 (0.9)	-	4.1	4.0	-	2.9 (1.7)	1.9 (0.8)	-	7.75	7.86	-	0.05	0.03	-	0.02	0.05	-	0.02	0.05
HD886	B2IV	-	23.3 (0.2)	21.7 (0.1)	-	3.9	3.9	-	3.9 (2.2)	1.6 (0.5)	-	7.53	7.77	-	0.03	0.01	-	0.02	0.05	-	0.06	0.07
HD253049	B2IV	-	20.8 (1.3)	19.7 (0.9)	-	3.8	3.8	-	3.2 (2.2)	4.1 (3.2)	-	7.48	7.66	-	0.05	0.09	-	0.08	0.08	-	0.06	0.10
HD60553	B2II	-	23.9 (1.0)	-	-	4.0	-	-	3.7 (2.8)	-	-	7.85	-	-	0.11	-	-	0.09	-	-	0.02	-
HD223128	B2IV	-	23.2 (0.8)	22.6 (0.3)	-	3.9	3.9	-	-	2.4 (1.4)	-	-	7.89	-	-	0.06	-	-	0.03	-	-	0.06
HD829	B3III	-	21.1 (0.3)	18.9 (0.2)	-	3.9	3.8	-	4.2 (2.5)	2.9 (2.0)	-	7.42	7.83	-	0.05	0.05	-	0.05	0.07	-	0.08	0.12
HD77770	B2IV	-	20.6 (1.0)	18.8 (0.5)	-	3.7	3.7	-	3.4 (2.5)	3.8 (3.0)	-	7.31	7.63	-	0.05	0.10	-	0.03	0.04	-	0.06	0.13
HD162374	B6Ib	-	18.0 (0.4)	16.6 (0.3)	-	3.7	3.7	-	5.8 (3.9)	4.2 (3.5)	-	7.72	8.16	-	0.09	0.11	-	0.06	0.03	-	0.14	0.17
HD174298	B1.5V	-	24.5 (1.0)	24.2 (1.2)	-	4.0	4.0	-	-	2.1 (1.0)	-	-	7.88	-	-	0.06	-	-	0.06	-	-	0.02
HD64365	B2III	-	23.3 (0.4)	22.6 (0.3)	-	3.8	3.8	-	2.1 (0.9)	2.5 (0.9)	-	8.13	8.19	-	0.05	0.05	-	0.06	0.06	-	0.03	0.05
HD158304	B3III	-	22.1 (0.7)	19.2 (0.3)	-	4.0	3.8	-	4.5 (4.0)	5.3 (4.1)	-	7.45	7.83	-	0.08	0.11	-	0.07	0.06	-	0.05	0.11
HD37356	B3V	-	24.0 (1.0)	21.8 (0.5)	-	4.0	3.8	-	11.8 (4.0)	5.8 (4.5)	-	7.52	7.68	-	0.02	0.08	-	0.04	0.03	-	0.03	0.10
HD220172	B3II	-	23.9 (0.7)	22.1 (0.7)	-	4.0	3.9	-	2.2 (1.2)	3.3 (2.5)	-	7.59	7.65	-	0.03	0.08	-	0.07	0.06	-	0.03	0.06
HD35299	B2III	23.5 (0.5)	24.4 (0.5)	23.0 (0.3)	4.1	4.1	4.1	2.5 (0.6)	1.7 (0.6)	3.0 (0.6)	7.76	7.72	7.80	0.02	0.02	0.02	0.05	0.05	0.05	0.04	0.02	0.03
HD197512	B2III	22.5 (1.0)	24.2 (0.6)	23.1 (2.0)	3.9	3.8	3.9	3.7 (1.2)	2.5 (1.0)	3.4 (1.0)	8.23	8.11	8.17	0.06	0.05	0.06	0.05	0.04	0.05	0.05	0.01	0.04
HD35337	B2III	23.2 (0.5)	24.6 (0.5)	22.7 (0.2)	4.0	4.1	4.0	1.7 (0.6)	1.1 (0.1)	1.5 (0.5)	7.76	7.72	7.74	0.03	0.00	0.03	0.02	0.03	0.03	0.04	0.01	0.04
HD43112	B2III	25.2 (0.6)	26.5 (0.2)	-	4.0	4.2	-	2.6 (0.8)	2.4 (0.8)	-	7.86	7.96	-	0.03	0.03	-	0.05	0.07	-	0.04	0.02	-
CPD573524B	B1V	24.3 (1.4)	-	-	3.8	-	-	6.4 (2.3)	-	-	7.61	-	-	0.08	-	-	0.09	-	-	0.01	-	-
HD205021	B0.5IIIs	25.8 (0.5)	-	-	3.8	-	-	1.9 (0.5)	-	-	7.98	-	-	0.02	-	-	0.07	-	-	0.04	-	-
HD36591	B2II/III	26.2 (0.2)	-	-	3.9	-	-	1.5 (0.5)	-	-	7.72	-	-	0.01	-	-	0.07	-	-	0.04	-	-
HD36960	B1/2Ib/II	27.5 (0.4)	-	-	3.8	-	-	5.5 (4.0)	-	-	7.53	-	-	0.06	-	-	0.08	-	-	0.06	-	-
HD201795	B1V	28.6 (0.1)	-	-	4.1	-	-	2.1 (0.6)	-	-	7.66	-	-	0.01	-	-	0.04	-	-	0.03	-	-
HD34816	B0.5V	28.8 (0.4)	-	-	3.9	-	-	6.1 (3.4)	-	-	7.55	-	-	0.09	-	-	0.12	-	-	0.06	-	-
HD36822	B0III	29.3 (0.3)	-	-	3.8	-	-	4.6 (2.5)	-	-	7.90	-	-	0.07	-	-	0.12	-	-	0.07	-	-
HD119069	B3II	28.8 (0.4)	-	-	4.0	-	-	5.8 (3.2)	-	-	7.67	-	-	0.06	-	-	0.10	-	-	0.05	-	-
HD149438	B0.2V	31.1 (0.1)	-	-	4.0	-	-	3.2 (0.5)	-	-	8.10	-	-	0.01	-	-	0.05	-	-	0.06	-	-
HD202214	O9.5IV	28.6 (0.5)	-	-	3.7	-	-	2.3 (1.3)	-	-	7.71	-	-	0.02	-	-	0.08	-	-	0.04	-	-
HD46328	B0.7IV	25.8 (0.1)	-	-	3.7	-	-	2.9 (0.5)	-	-	8.02	-	-	0.02	-	-	0.07	-	-	0.05	-	-
HD61068	B2II	25.5 (0.4)	-	-	4.0	-	-	2.0 (0.8)	-	-	7.96	-	-	0.04	-	-	0.10	-	-	0.03	-	-
HD36512	O9.7V	32.6 (0.3)	-	-	4.0	-	-	5.3 (2.8)	-	-	7.69	-	-	0.03	-	-	0.22	-	-	0.16	-	-
HD166523	B3II	27.2 (1.0)	-	-	4.0	-	-	2.2 (1.1)	-	-	7.93	-	-	0.04	-	-	0.05	-	-	0.04	-	-
HD59882	B2Ib/II	25.0 (0.4)	-	-	3.8	-	-	2.9 (0.8)	-	-	8.24	-	-	0.05	-	-	0.14	-	-	0.02	-	-
HD255134	B1IVp	26.4 (0.1)	-	-	3.7	-	-	4.6 (5.0)	-	-	7.46	-	-	0.07	-	-	0.03	-	-	0.04	-	-
HD34989	B1V	26.1 (0.8)	-	-	4.1	-	-	2.1 (1.0)	-	-	7.68	-	-	0.03	-	-	0.10	-	-	0.03	-	-
HD37209	B3IV	26.2 (0.6)	-	-	3.9	-	-	6.5 (2.3)	-	-	7.66	-	-	0.03	-	-	0.09	-	-	0.01	-	-

Star Name	Spec Typ	T_{eff} [$\cdot 10^3$ K]			Logg			ξ(Microturbulence)			Log(N/H)+12 [dex]			ΔLog(N/H)$_\xi$ [dex]			ΔLog(N/H)$_{dis}$ [dex]			ΔLog(N/H)$_T$ [dex]		
		A	B	C	A	B	C	A	B	C	A	B	C	A	B	C	A	B	C	A	B	C
HD54025	B2II	24.8 (1.0)	-	-	4.1	-	-	2.5 (1.8)	-	-	7.55	-	-	0.04	-	-	0.07	-	-	0.04	-	-
HD129557	B2III	23.6 (1.0)	-	-	3.9	-	-	2.0 (0.8)	-	-	8.55	-	-	0.05	-	-	0.08	-	-	0.03	-	-
HD251847	B1IV	28.4 (1.2)	-	-	3.8	-	-	12.1 (2.3)	-	-	7.59	-	-	0.03	-	-	0.15	-	-	0.01	-	-
HD201638	B0.5Ib	25.3 (1.0)	-	-	3.7	-	-	6.3 (4.3)	-	-	8.3	-	-	0.24	-	-	0.11	-	-	0.03	-	-
HD211880	B0.5V	30.4 (0.9)	-	-	4.1	-	-	4.4 (3.5)	-	-	7.94	-	-	0.08	-	-	0.13	-	-	0.05	-	-
HD164704	B2II	26.3 (0.7)	-	-	4.1	-	-	2.9 (1.9)	-	-	7.69	-	-	0.06	-	-	0.05	-	-	0.03	-	-
HD165016	B2Ib	30.2 (0.4)	-	-	3.9	-	-	2.1 (1.0)	-	-	7.75	-	-	0.01	-	-	0.07	-	-	0.07	-	-
HD192039	B0IV	31.8 (0.4)	-	-	3.8	-	-	5.4 (4.1)	-	-	7.91	-	-	0.05	-	-	0.07	-	-	0.10	-	-
HD166539	B1/2Ib	32.8 (0.7)	-	-	3.8	-	-	2.2 (0.7)	-	-	7.96	-	-	0.01	-	-	0.10	-	-	0.19	-	-
HD34078	O9.5V	34.1 (0.3)	-	-	4.0	-	-	4.5 (2.7)	-	-	7.74	-	-	0.02	-	-	0.20	-	-	0.13	-	-
HD206183	O9.5IV-V	33.5 (0.3)	-	-	4.0	-	-	4.2 (2.7)	-	-	7.89	-	-	0.03	-	-	0.21	-	-	0.13	-	-
HD161789	B2/3II	33.0 (0.6)	-	-	4.1	-	-	1.7 (0.6)	-	-	7.75	-	-	0.01	-	-	0.15	-	-	0.05	-	-

A.3. Variability and binarity

Table A.3.: This Table presents the results obtained with the analysis of TESS light curves and periodograms. Second column shows the variability magnitude of the light curve. Frequency values are in the third column, which is divided into three subcolumns: the first one to indicate if the star is SLF (Stochastic Low Frequency), second one to show frequencies of peaks in g-mode, and third one to show frequencies of peaks in p-mode. Some of the stars had more than one light curve available so, in those cases, Table shows all the magnitude and frequency values for each light curve of the star. The fourth column indicates if any contaminant might be affecting the photometric values from TESS. The Fifth column shows the classification of the star according to the binarity.

Star Name	σ(**T**$_P$) **[mmag]**	**Frequency [cycles/day]**					**Contaminants**	**Binarity**
		SLF	**g-mode (f<1)**		**p-mode (f>1)**			
			f [cycles/day]	**Amp**	**f [cycles/day]**	**Amp**		
HD85953	7.80366	NO	0.265543	1	-	-	-	LS(2)
	6.46126	NO	0.263851	1	-	-		
	7.97412	NO	0.2679	1	-	-		
HD3360	1.44137	NO	0.16506	1	3.66364	0.8	NO	LS(2)
HD35039	2.44177	NO	0.357011 0.26674 0.50962	1 0.61 0.54	-	-	-	SBI(12)
HD42690	2.73695	NO	0.494821	1	-	-	NO	LS(2)
	2.88848	NO	0.535912 0.662523 0.346069	1 0.87 0.6	-	-		
HD157056	-	-	-	-	-	-	NO	LS(2)
HD886	4.19659	NO	-	-	6.58964 6.5305 6.64864	1 0.63 0.63	NO	LS(7)
HD253049	1.94901	YES	0.295214	1	-	-	NO	LS(8)
	2.13364	YES	0.297463	1	-	-		
	1.8559	YES	0.296131	1	-	-		
HD60553	-	-	-	-	-	-	NO	LS(3)
HD223128	2.5527	NO	0.56722	1	7.71665	0.37	-	-
	2.25812	NO	0.55859	1	7.71824	0.4		
	2.43008	NO	0.560085	1	7.71704	0.35		

Star Name	TESS Std	Frequency [cycles/day]					Contaminants	Binarity
		SLF	g-mode (f<1)		p-mode (f>1)			
			f [cycles/day]	Amp	f [cycles/day]	Amp		
HD162374	4.0282	NO	0.399641	1	-	-	-	-
			0.196292	0.76				
HD174298	5.09066	NO	-	-	10.2569	1	-	-
	5.08012	NO	-	-	10.2572	1		
HD64365	6.5913	NO	-	-	4.96013	1	-	-
					5.36881	0.85		
					5.18311	0.51		
	7.03563	NO	-	-	4.96143	1		
					5.36516	0.96		
					5.1814	0.55		
	7.33871	NO	-	-	4.96031	1		
					5.37046	0.77		
					5.18286	0.6		
	6.98828	NO	-	-	4.96022	1		
					5.3692	0.82		
					5.1854	0.65		
HD158304	-	-	-	-	-	-	NO	LS(2)
HD37356	0.220554	YES	0.369915	1	-	-	-	-
			0.141117	0.87				
			0.273315	0.66				
HD220172	0.825008	NO	0.615841	1	-	-	NO	LS(9)
HD35299	1.07198	NO	0.791993	0.94	1.26453	1	NO	LS(3)
			0.672094	0.89	1.0546	0.69		
HD197512	1.136210	NO	0.796301	1	-	-	NO	LS(3)
			0.347466	0.95				
			1.00702	0.6				
HD35337	-	-	-	-	-		SP	SBI(3)
HD43112	0.243839	YES	0.319647	1	-	-	NO	LS(2)
	0.205137	YES	0.180813	1	-	-		
	0.194425	YES	0.467505	1	-	-		
	0.234152	YES	0.184264	1	-	-		
	0.217383	YES	0.296018	1	-	-		
CPD573524B	12.84520	NO	-	-	5.60712	1	YES VS	SBI(4)
					5.68692	0.8		
	12.65670	NO	-	-	5.60189	1		
					5.6965	0.82		

Star Name	TESS Std	Frequency [cycles/day]					Contaminants	Binarity
		SLF	g-mode (f<1)		p-mode (f>1)			
			f [cycles/day]	Amp	f [cycles/day]	Amp		
HD205021	10.92670	NO	-	-	5.24982	1	YES	SBI(2)
					10.4999	0.18		
	10.77100	NO	-	-	5.24962	1		
					10.4985	0.17		
	10.50850	NO	-	-	5.24935	1		
					10.4994	0.19		
	10.07560	NO	-	-	5.24922	1		
					10.4991	0.19		
	10.21400	NO	-	-	5.24945	1		
					10.4995	0.18		
HD36591	0.219693	YES	0.249957	1	-	-	NO	LS(3)
			0.367315	0.87				
	0.199416	YES	0.191581	1	-	-		
			0.516127	0.65				
HD36960	0.635910	YES	0.293196	1	-	-	YES	LS(5)
	0.509401	YES	0.746011	1	-	-		
HD34816	1.184700	NO	0.791905	1	1.58514	0.28	NO	LS(67)
	1.200620	NO	0.792765	1	1.58543	0.29		
HD36822	0.569654	NO	0.885081	1	1.76585	0.35	NO SP	SBI(3)
HD149438	1.271310	YES	0.200518	1	-	-	NO	LS(28)
	0.100618	YES	0.235448	1	-	-		
HD202214	0.791339	YES	0.472279	1	5.98990	0.83	YESDou/mult	SBII(26)
					8.11949	0.48		
	0.881260	YES	0.170065	1	5.98959	0.98		
					8.11757	0.53		
HD46328	9.116410	NO	-	-	4.77154	1	YES	SBI(3)
					9.54167	0.16		
	9.557820	NO	-	-	4.77147	1		
					9.54279	0.14		
HD61068	6.403930	NO	-	-	6.07235	1	Variable	SBI(3)
					6.45131	0.35		
	6.793210	NO	-	-	5.99504	1		
					6.45338	0.39		
HD36512	0.163852	YES	0.227776	1	12.71170	0.70	Spec binary	-
	0.137193	YES	0.146497	1	12.70460	0.34		
HD166523	-	-	-	-	-	-	NO	SBI (2)
HD59882	0.652502	YES	0.115955	1	-	-	-	-
HD37209	0.259411	NO	0.274104	1	7.82637	0.70	NO	LS(4)
					6.48824	0.65		

Star Name	TESS Std	Frequency [cycles/day]					Contaminants	Binarity
		SLF	g-mode (f<1)		p-mode (f>1)			
			f [cycles/day]	Amp	f [cycles/day]	Amp		
HD255134	0.754130	YES	0.357144	1	-	-	YES	SBI(6)
	0.860465	YES	0.291720	1	-	-		
	0.823856	YES	0.290059	1	-	-		
HD34989	0.212730	NO	0.796525	1	-	-	NO	SBI(5)
HD129557	6.829150	NO	-	-	7.83801	1	-	-
					8.00657	0.58		
					7.43528	0.50		
	7.030150	NO	-	-	7.83930	1		
					8.00457	0.69		
					7.43729	0.48		
HD251847	0.685925	YES	0.438415	0.61	5.47342	1	YES	LS(2)
					1.99932	0.45		
HD201638	-	-	-	-	-	-	YES	LS(3)
HD211880	-	-	-	-	-	-	YES	LS(2)
HD165016	-	-	-	-	-	-	NO	SBI(2)
HD192039	0.600657	YES	0.172582	1			-	-
HD34078	0.374606	YES	0.176093	1	-	-	YVariable	SBII(78)
	0.868456	YES	0.110759	1	-	-		
	0.303556	YES	0.257337	1	-	-		
	0.418028	YES	0.338971	1	-	-		
HD206183	-	-	-	-	-	-	YES	LS(2)